Analytical Biochemistry 508 (2016) 78–96

Contents lists available at ScienceDirect

Analytical Biochemistry

journal homepage: www.elsevier.com/locate/yabio

Comparison of biosensor platforms in the evaluation of high affinity antibody-antigen binding kinetics

Danlin Yang [a, 1], Ajit Singh [a, b, 1], Helen Wu [a], Rachel Kroe-Barrett [a, *]

[a] Department of Immune Modulation and Biotherapeutics Discovery, Boehringer Ingelheim Pharmaceuticals, Inc., Ridgefield, CT 06877, USA
[b] The Fu Foundation School of Engineering and Applied Science, Columbia University, New York, USA

ARTICLE INFO

Article history:
Received 19 April 2016
Received in revised form
15 June 2016
Accepted 24 June 2016
Available online 27 June 2016

Keywords:
Biacore
ProteOn
Octet
MX96
Antibody-antigen interactions
Optical biosensor

ABSTRACT

The acquisition of reliable kinetic parameters for the characterization of biomolecular interactions is an important component of the drug discovery and development process. While several benchmark studies have explored the variability of kinetic rate constants obtained from multiple laboratories and biosensors, a direct comparison of these instruments' performance has not been undertaken, and systematic factors contributing to data variability from these systems have not been discussed. To address these questions, a panel of ten high-affinity monoclonal antibodies was simultaneously evaluated for their binding kinetics against the same antigen on four biosensor platforms: GE Healthcare's Biacore T100, Bio-Rad's ProteOn XPR36, ForteBio's Octet RED384, and Wasatch Microfluidics's IBIS MX96. We compared the strengths and weaknesses of these systems and found that despite certain inherent systematic limitations in instrumentation, the rank orders of both the association and dissociation rate constants were highly correlated between these instruments. Our results also revealed a trade-off between data reliability and sample throughput. Biacore T100, followed by ProteOn XPR36, exhibited excellent data quality and consistency, whereas Octet RED384 and IBIS MX96 demonstrated high flexibility and throughput with compromises in data accuracy and reproducibility. Our results support the need for a "fit-for-purpose" approach in instrument selection for biosensor studies.

Introduction

The characterization of antibody-antigen interactions is essential for the successful development of antibody-based therapeutics. Label-free optical surface plasmon resonance (SPR) biosensors, the gold standard for measuring the binding affinity and kinetics of molecular interactions, are used across multiple stages of drug discovery and development [1–3]. SPR biosensors have been used to characterize antibody-antigen interactions for approximately two decades [4–6], with applications ranging from the low-resolution affinity screening of antibody supernatants [7], to the rigorous, high-resolution kinetic constant determinations of purified antibodies [8], and the classification of antibody binding epitopes via epitope binning studies [9]. The availability of high-quality binding data enables the early selection of criteria-meeting drug candidates and provides crucial information for pharmacokinetic/pharmacodynamic modeling in the design of clinical dosing strategies [10].

With the rapidly expanding use of monoclonal antibodies (mAbs) and antibody-like scaffolds for various therapeutic indications [11,12], the demand for the efficient, rapid and accurate identification of therapeutic candidates that meet specific

abbreviations: mAb, monoclonal antibody; SPR, surface plasmon resonance; BLI, Bio-Layer Interferometry; CFM, continuous flow microfluidics; PCSK9, proprotein convertase substilisin kexin type 9; EDC, 1-ethyl-3-(3-dimethylaminopropyl)carbodiimide hydrochloride; NHS, *N*-hydroxysuccinimide; sulfo-NHS, *N*-hydroxysulfocussinimide; EDTA, ethylenediaminetetraacetic acid; CHO, Chinese hamster ovary; Ni-NTA, nickel-nitrilotriacetic acid; SEC, size exclusion chromatography; UPLC, ultra-performance liquid chromatography; k_a, association rate constant; k_d, dissociation rate constant; K_D, equilibrium dissociation constant; RU, response unit; R_{max}, maximal binding response; R_L, ligand response.

* Corresponding author. Department of Immune Modulation and Biotherapeutics Discovery, Boehringer Ingelheim Pharmaceuticals, Inc., 900 Ridgebury Road, Ridgefield, CT 06877-0368, USA
E-mail address: rachel.kroe-barrett@boehringer-ingelheim.com (R. Kroe-Barrett).
[1] Contributed equally to this work.

http://dx.doi.org/10.1016/j.ab.2016.06.024

requirements has dramatically increased. During recent years, a wide variety of innovative instruments have been developed to address this increasing demand, many of which have demonstrated significant throughput improvements over the traditional Biacore SPR platform [13]. These instruments differ in either the design of microfluidic channel configurations and/or the optical principles in the detection of bimolecular interactions. Examples include the 6 × 6 crisscross microfluidics configuration in Bio-Rad's ProteOn XPR36, the 96-microarray printing by the Continuous Flow Microspotter (CFM) in Wasatch Microfluidics's IBIS MX96 [14,15], and the BioLayer Interferometry (BLI) optical detection technique in ForteBio's Octet RED384 [16] that is coupled to a 384-well high-throughput format. While the well-established SPR-based (GE Healthcare's Biacore T100 and Bio-Rad's ProteOn XPR36) and BLI-based (ForteBio's Octet RED384) platforms are widely used by many laboratories worldwide, the Wasatch Microfluidics's IBIS MX96 instrument is relatively new to the biosensor field. The IBIS MX96 operates based on the SPR imaging (SPRi) sensor technology that provides detection in spatial orientation – which the regular SPR cannot, thus enabling multiplex imaging of ligand surfaces in an array format [15]. Collectively, researchers now have a number of instruments to choose from for their biosensor studies.

Although these various biosensor platforms all provide kinetic data that is essential for characterizing molecular interactions, they are costly investments. For new users with little hands-on biosensor experience, the decision of which instrument to purchase can often be a challenging task given the many factors to consider, including data quality, performance consistency, throughput, ease of operation, and material consumption, all of which must often be balanced against cost. To ensure that users select the instrument that can deliver the most reliable results for the intended applications, it is important for them to be aware of each instrument's strengths and weaknesses prior to purchase. While past benchmark studies have explored the variability in reported kinetic rate constants across laboratories and instruments [8,17], a comprehensive comparison of the various biosensor platforms has not been conducted.

With the availability of the four routinely used biosensor platforms in our laboratory (the Biacore T100, ProteOn XPR36, Octet RED384, and IBIS MX96), we performed a head-to-head comparison study using a panel of high-affinity mouse-derived monoclonal antibodies against human proprotein convertase substilisin kexin type 9 (PCSK9). Our goals were to determine the effect of instrumental performance on data quality and variability, and to help guide the selection of appropriate platforms for antibody-antigen studies in drug discovery research. We compared the experimental details of each instrument, from ligand surface uniformity to analyte binding analysis, and discussed the strength and weaknesses of each biosensor platform with an emphasis on data consistency, comparability, and operational efficiency.

Materials and methods

Proteins and antibodies

Suspension HEK293-6E cells were transfected with plasmid DNA encoding C-terminally 6-His-tagged human PCSK9 using the TransIT-PRO system (Mirus Bio LLC). The transfected cells were incubated for 4 days, and then the medium was harvested and used to purify the 6-His-tagged PCSK9 with a Ni-NTA His-Bind Superflow column (Novagen) following the manufacturer's instructions.

CHO cells were transfected with plasmid DNAs containing heavy chain and light chain cassettes using Freestyle CHO Expression Medium with 8 mM Glutamax (Invitrogen). The transfected cells were incubated for 7 days, and then the medium was harvested and used to purify the antibodies with the ÄKTA affinity chromatography system and MabSelect Sure resin (GE Healthcare) following standard methods [18]. The purified mAbs were formulated in 60 mM sodium acetate (pH 5.0), and their concentrations were determined by adsorption at 280 nm using an extinction coefficient of 1.36 [18] in NanoDrop™ 8000 Spectrophotometer (Thermo Fischer Scientific). Their purities were subsequently assessed to be >95% monomer by size exclusion ultra-performance liquid chromatography (UPLC) (ACQUITY, Waters Corporation).

Instruments and reagents

The binding experiments were performed on four biosensors, the Biacore T100, ProteOn XPR36, Octet RED384, and IBIS MX96. The Biacore T100, equipped with CM5 sensor chips, was purchased from GE Healthcare (Piscataway, NJ, USA) and the ProteOn XPR36, equipped with a GLM sensor chip, was purchased from Bio-Rad (Hercules, CA, USA). The Octet RED384, equipped with AHC (anti-Human IgG Fc capture) biosensor tips was purchased from ForteBio (Menlo Park, CA, USA), and the IBIS MX96, supplied with a CFM printer and SensEye COOH-G chip was purchased from Wasatch Microfluidics (Salt Lake City, UT, USA). Recombinant protein A/G was purchased from Thermo Fischer Scientific (catalog # 21186). To couple the protein A/G to the biosensor surfaces, we used an amine coupling kit consisting of 10 mM sodium acetate (pH 4.5), 200 mM 1-ethyl-3-(3-dimethylaminopropyl)carbodiimide hydrochloride (EDC), 50 mM *N*-hydroxysuccinimide (NHS), and 1 M ethanolamine-HCl (pH 8.5) (GE Healthcare, product # BR1000050) and the ProteOn amine coupling kit containing 400 mM EDC, 100 mM *N*-hydroxysulfosuccinimide (sulfo-NHS), and 1 M ethanolamine-HCl (pH 8.5) (Bio-Rad, catalog # 1762410). Various regeneration solutions, including 4 M $MgCl_2$, 10 mM glycine-HCl pH 2.5, pH 2.0, and pH 1.5 (GE Healthcare), and 0.85% phosphoric acid (Bio-Rad) stock diluted at 1/500 (v/v) in water were tested.

Biacore T100 kinetic measurements

Protein A/G was immobilized onto the 4 individual flow cells in the CM5 sensor chip using a standard coupling protocol. First, the carboxyl groups on the sensor surface were activated by injecting a fresh mixture of EDC/NHS (200 mM/50 mM), and then protein A/G prepared at 30 μg/mL in sodium acetate (pH 4.5) was injected over the activated surface, and the protein was covalently attached by its primary amines. Finally, the excess reactive esters were blocked with 1 M ethanolamine. Each step was performed with a 7-min injection at a 5 μl/min flow rate. For the subsequent antibody-capturing step, the flow rate was increased to 10 μl/min. Each mAb, prepared at 0.063 μg/mL in HBS-EP (10 mM HEPES [pH 7.4], 150 mM NaCl, 3 mM EDTA, and 0.005% v/v polysorbate P20) running buffer, was injected serially onto flow cells 2, 3, and 4 using programmed times of 220 s, 110 s, and 55 s, respectively. Flow cell 1 was left empty to provide a reference surface. To measure the binding kinetics, human PCSK9 from 100 nM to 0.39 nM in 2-fold serial dilutions, as well as a blank buffer for baseline subtraction were injected sequentially with a regeneration step inserted between each cycle. Regeneration of the protein A/G surface was achieved with two 18-sec pulses of glycine (pH 1.5) at 50 μl/min. The binding interactions were monitored in running buffer over a 10-min association period and a 45-min dissociation period at 30 μl/min.

ProteOn XPR36 kinetic measurements

Similar coupling procedures were used to immobilize protein A/G onto the GLM sensor chip imprinted with 6 crisscrossing flow

channels. Instead of using NHS in the activation step, 100 mM sulfo-NHS was used in combination with 400 mM EDC. Each activation, immobilization, and deactivation step was carried out for 5 min with 6 parallel injections in the horizontal direction at 30 μl/min. The prepared protein A/G surfaces were subsequently conditioned with three 18-sec pulses of glycine (pH 1.5) at 100 μl/min in both the horizontal and vertical directions. Two different mAbs, each prepared at 0.25 μg/mL, 0.125 μg/mL, and 0.063 μg/mL in PBS-T-EDTA (PBS [pH 7.4], 0.005% Tween-20, and 3 mM EDTA) running buffer were then injected in parallel in the vertical direction for 160 s at 25 μl/min. Channels 1–3 were injected with one mAb, and channels 4–6 were injected with the other. Following a switch in orientation of the sensor chip and a blank buffer injection of 60 s, the antigen binding kinetics of the mAbs in the six samples was measured by injecting 5 concentrations of human PCSK9, together with a blank buffer, simultaneously. Three different series of human PCSK9 concentrations (100 nM–6.25 nM, 25 nM–1.56 nM, and 5 nM–0.313 nM) were prepared by 2-fold serial dilution. The binding interactions were monitored in running buffer over a 10-min association period and a 45-min dissociation period at 40 μl/min. After each binding cycle, the protein A/G surface was regenerated with two 18-sec pulses of glycine (pH 1.5) at 100 μl/min in both the horizontal and vertical directions.

Octet RED384 kinetic measurements

Each mAb prepared at 20 μg/mL, 10 μg/mL, and 5 μg/mL in 1 × KB (PBS pH [7.4], 0.02% Tween-20, 0.1% albumin, and 0.05% sodium azide) running buffer was dispensed into a 384-well tilted-bottom microplate at a volume of 90 μl per well. Each concentration occupied 8 vertical wells. A second 384-well microplate containing human PCSK9 at 7 titrated concentrations (100 nM–1.56 nM, in 2-fold serial dilutions), the glycine [pH 1.5] regeneration solution, and 1 × KB buffer for baseline stabilization was also prepared. Both plates were agitated at 1000 rpm over the entire course of the experiment. A total of 16 AHC (anti-human Fc capture) sensor tips were used for a group of 2 mAbs (8 sensors each) per binding cycle. Prior to the binding measurements, the sensor tips were pre-hydrated in 1 × KB for 5 min, followed by 3 cycles of pre-conditioning with 15-sec dips in glycine (pH 1.5), alternating with 15-sec dips in 1 × KB. The sensor tips were then transferred to the mAb-containing wells for a 200-sec loading step. After a 60-sec baseline dip in 1 × KB, the binding kinetics were measured by dipping the mAb-coated sensors into the wells containing human PCSK9 at varying concentrations. The binding interactions were monitored over a 500-sec association period and followed by a 30-min dissociation period in new wells containing fresh 1 × KB buffer. The AHC sensor tips were regenerated with two 18-sec dips in glycine (pH 1.5) between each binding cycle.

IBIS MX96 kinetic measurements

Multi-cycle kinetics with amine-coupled antibody arrays

For multi-array printing of the CFM, two 96-well microplates were prepared. The sample source plate contained 8 vertical wells of each mAb prepared in sodium acetate (pH 5.0) from 20 μg/mL to 0.16 μg/mL in 2-fold serial dilutions, and the reagent plate contained freshly prepared EDC/sulfo-NHS (400 mM/100 mM). After the COOH-G SensEye chip in the CFM was primed with sodium acetate (pH 5.0) running buffer, the sensor surface was activated with the EDC/sulfo-NHS mixture for 5 min, followed by the immobilization of mAbs directly onto the activated surface. During this step, the mAb samples in the top half of the source plate were delivered to the sensor using 48 micro-channels, which allowed the samples to cycle across the activated surfaces bidirectionally for 10 min. The procedure was repeated for the remaining mAb samples in the bottom half of the source plate, resulting in the generation of a 10 × 8 array of mAb spots on the sensor surface. Two vertical columns of wells contained only buffer, which served as reference samples. The printed sensor chip was then docked into the MX96 instrument and primed with the system's running buffer (PBS [pH 7.4], 0.01% Tween-20) before quenching the surfaces with 1 M ethanolamine for 5 min. The binding interactions were measured by cycling human PCSK9 prepared in the system running buffer at 9 concentrations (0.39–100 nM in 2-fold serial dilutions) across the mAb array surface. The cycling of each sequentially injected sample was monitored for a 10-min association period followed by a 45-min dissociation period, at a flow rate of 40 μl/min. Regeneration of the amine-coupled mAb surfaces using glycine (pH 2.0 or pH 2.5) solutions was performed between each binding cycle. These regeneration conditions were chosen based on a preliminary experiment.

Single-cycle kinetics with Fc-captured antibody arrays

A SensEye COOH-G chip was first docked into the MX96 instrument and primed with sodium acetate (pH 5.0) running buffer. The sensor surface was activated by injecting EDC/sulfo-NHS (400 mM/100 mM) for 5 min, then protein A/G prepared at 50 μg/mL in the running buffer was bidirectionally cycled across the activated surface for 5 min. The sensor chip with the immobilized protein A/G surface was then removed from the MX96 and inserted into the CFM printer, which had been loaded with a 96-well mAb source plate. The same plate layout and mAb concentrations described above for the amine-coupled antibody array were used, but the mAbs were prepared in the system running buffer, which was PBS and 0.01% Tween-20. After the mAb samples were captured through cycling across the protein A/G surface for 10 min, the sensor chip was docked back into the MX96 instrument and primed with the system running buffer. The binding interactions were measured by cycling human PCSK9 prepared in the system running buffer at 7 concentrations (1.56 nM–100 nM in 2-fold serial dilutions). The cycling of each sequentially injected sample was monitored as described in the previous section. No regeneration was performed between sample injections.

Data analysis

Data processing and curve fitting

All of the binding sensorgrams were collected at 25 °C. Prior to curve-fitting analysis, the acquired data were processed as follows. The Biacore T100 data were double-referenced using reference flow cell 1 and preceding buffer blank subtraction using BiaEvaluation (v.4.1) and the ProteOn XPR36 data were double-referenced using channel inter-spots and a parallel in-line buffer blank subtraction by the integrated ProteOn Manager software (v.3.1.0.6). Octet RED384 data were referenced using a parallel buffer blank subtraction, and the baseline was aligned to the y-axis and smoothed by a Savitzky-Golay filter in the data analysis software (v.9.0.0.4). The IBIS MX96 data were first inter-spot reference subtracted and y-axis aligned using the IBIS SPRint software (v.6.15.2.1) and then the calibrated data were exported to Scrubber (v.2.0c) for cropping, aligning, and buffer injection referencing.

The processed binding curves from the four instruments were all fitted using the Langmuir model describing a 1:1 binding stoichiometry. In the Biacore T100, “single mode” was used to perform the fitting of individual mAb surfaces, whereas “batch mode” with “local” R_{max} was used to perform the global fitting of multiple mAb surfaces. Similarly, in the ProteOn XPR36, “grouped” and “global” modes were used along with “local” R_{max} in the fitting of single vs. multiple surfaces. In the Octet RED384, “R_{max} linked” was used to

perform the group fitting on sensors coated with the same mAb concentration, whereas "R_{max} unlinked by sensor" was used to perform the global fitting on sensors coated with multiple mAb concentrations. Both multi-cycle and single-cycle kinetic data from the IBIS MX96 were analyzed using Scrubber (v.2.0c). After the initial fitting of k_d in the absence of k_a, $k_a k_d$ was selected to fit with k_d being fixed, and the fit was then further refined by floating the k_d. For single-cycle kinetic data, the injection start time was set as a floating parameter to fit the association profiles back to a theoretical baseline origin. In all of the analyses, k_a is the association rate constant for the antibody-antigen binding reaction, k_d is the dissociation rate constant of the antibody-antigen complex, and K_D is the equilibrium dissociation constant defined by k_d/k_a. The accuracy of fitting is described by Chi^2 (Biacore T100, ProteOn XPR36, and IBIS MX96) or X^2 (Octet RED384), a parameter that represents how well the results approximate those calculated from the model used to analyze the data.

Ligand surface activity

The binding activity of surface-bound mAbs toward human PCSK9, namely the % ligand activity, was calculated using the following equations:

$$\%\ Ligand\ Activity = \frac{Experimental\ R_{max}}{Theoretical\ R_{max}} \times 100\%$$

where the theoretical R_{max} was determined as follows:

$$Theoretical\ R_{max} = \frac{Analyte\ MW}{Ligand\ MW} \times R_L \times S_M$$

where MW was the molecular weight of the ligand (mAb, 150 kDa) and analyte (human PCSK9, 72.8 kDa), R_L (ligand response) was the amount of immobilized ligand in response units (RU), and S_M was the stoichiometry as defined by the number of binding sites on the ligand. Rearranging the equation provides the calculation of an appropriate ligand density to aim for in the experiments:

$$R_L = \frac{Ligand\ MW}{Analyte\ MW} \times R_{max} \times \frac{1}{S_M}$$

For the kinetic binding measurements, R_{max} was set at 50–200 RU.

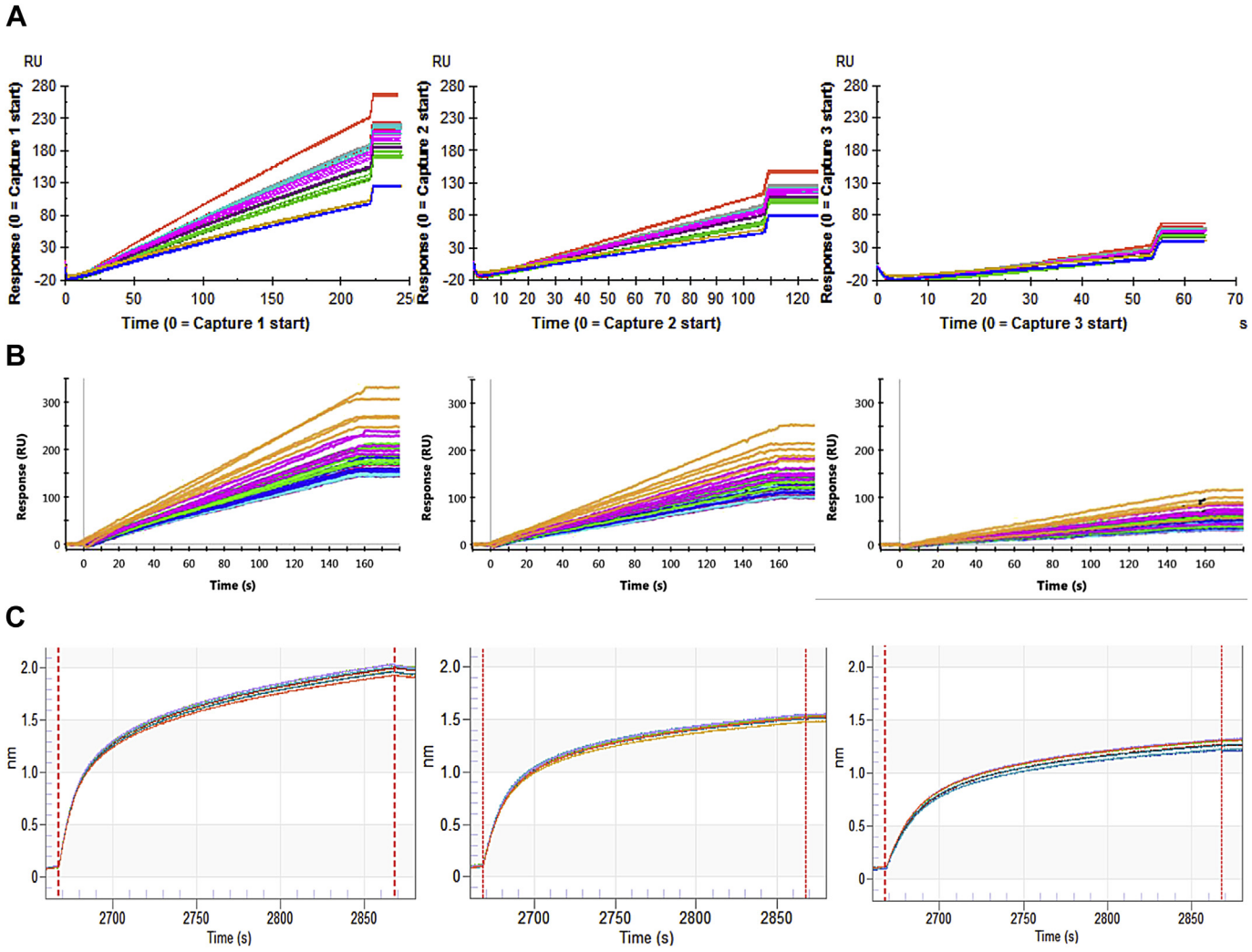

Fig. 1. Antibody capture levels on protein A/G immobilized surfaces in the Biacore T100 (A), ProteOn XPR36 (B), and Octet RED384 (C). Results from high- (*left*), medium- (*middle*), and low- (*right*) density surfaces are shown. The uniquely colored sensorgrams represent individual mAbs in (A), six ligand channels from multiple capture cycles in (B), and the simultaneous capture of a particular mAb at the same concentration by 8 AHC sensor tips in parallel in (C).

2.7.3. Correlation analysis

To compare the analyzed results of the ten mAbs across the four biosensor platforms, correlational (Spearman) analysis was performed on the kinetic rate and equilibrium binding constants relative to each other using GraphPad Prism (v6.05). The correlation coefficient (r) was determined along with the P-value, which represents the significance of the correlation.

Results

Ligand capture

In most cases, the mAbs were captured by protein A/G immobilized on the sensor surface. Protein A/G is commonly used in our laboratory as the capture reagent for IgGs due to its binding specificity towards the IgG Fc region of various species and subclasses [19]. Use of this protein therefore created a homogeneous orientation of the Fab regions on the sensor surface. We also made use of the anti-human IgG-Fc (AHC) sensor tips that were available for the Octet RED384, which allowed for direct Fc-mediated coating of the mAbs onto the sensor tips, without the need for surface preparation. To increase the rigor of the experiments, each mAb was analyzed at a minimum of three surface densities. For the Biacore T100 and ProteOn XPR36 experiments, we controlled the antibody contact times and concentrations, respectively, to generate a range of low- (~50 RU) to high-density (~250 RU) surfaces (Fig. 1A, B). These R_L levels were chosen based on the standard calculation of set R_{max} values as described in Materials and Methods. On the other hand, for the Octet RED384 and IBIS MX96 experiments, the mAb capture levels were achieved empirically by using a series of 2-fold serially diluted antibodies at constant times. While the low to high-density antibody capturing in the Octet RED384 was monitored in real-time, resulting in 1.0–2.0 nm wavelength shifts (Fig. 1C), the readout of mAb spots from the CFM was visualized through a camera in the MX96 and quantified based on the difference in bulk refractive index shifts between the amine-coupled (Fig. 2A) or Fc-captured (Fig. 2B) antibodies and their respective reference samples. As shown, a series of ten titrated mAbs was analyzed on each chip. However, quantitative comparisons of the printed R_L levels and the applied mAb concentrations indicated that they were not positively correlated and suggested that the samples were not printed consistently on the arrays.

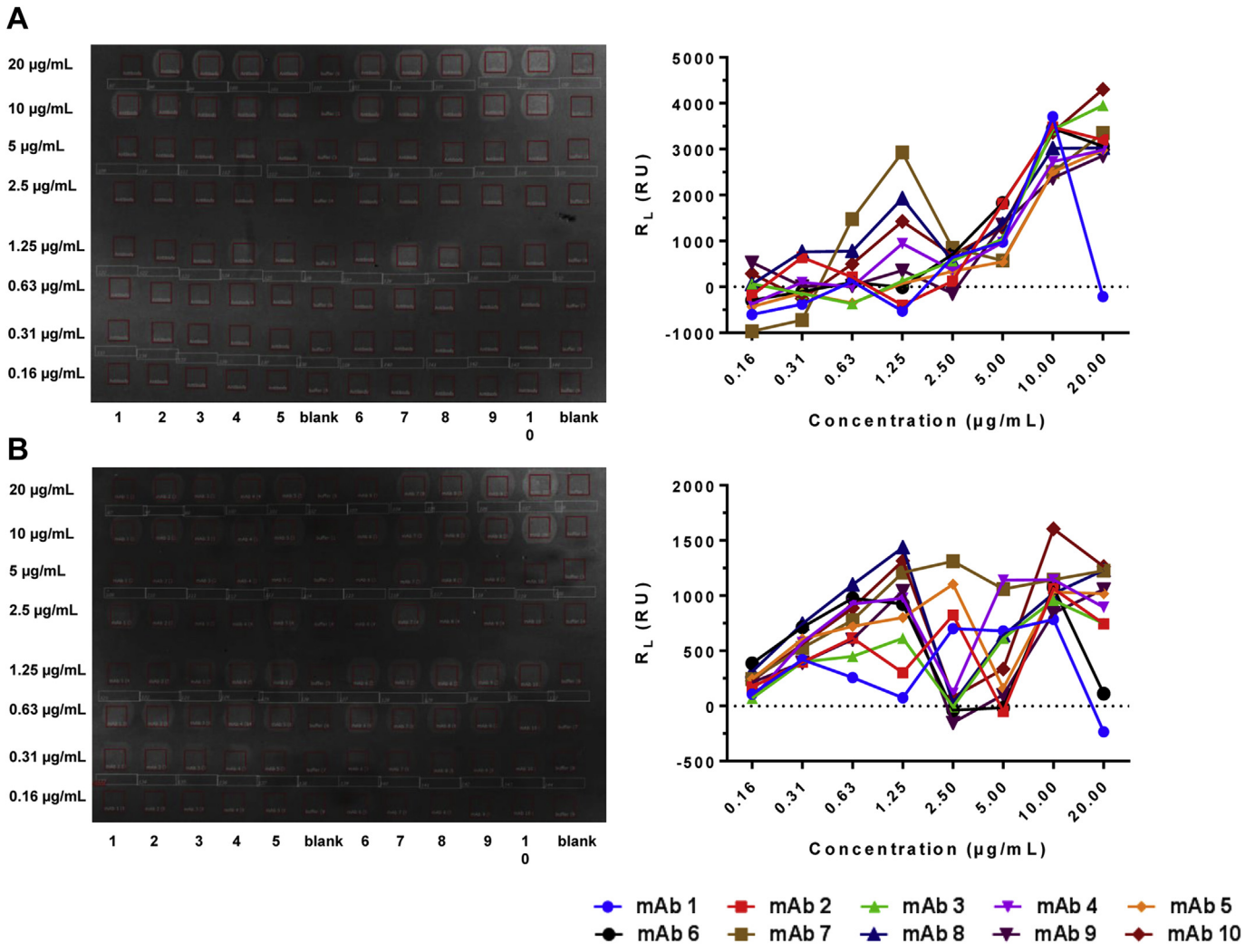

Fig. 2. CFM printing of antibody arrays and quantification of R_L levels of amine-coupled (A) and Fc-captured (B) antibody surfaces. The printed antibody spots are shown in the *left* panels, where the grey areas enclosed by red squares signify the presence of antibody. The darker inter-spots located between the active antibody spots were used for referencing. The printed antibody spots were quantified using the IBIS SPRint software by calculating the difference in bulk shifts between the active and reference locations (*right* panels). The antibodies are identified in the legend, and the number associated with each antibody corresponds to a number in the CFM array printout.

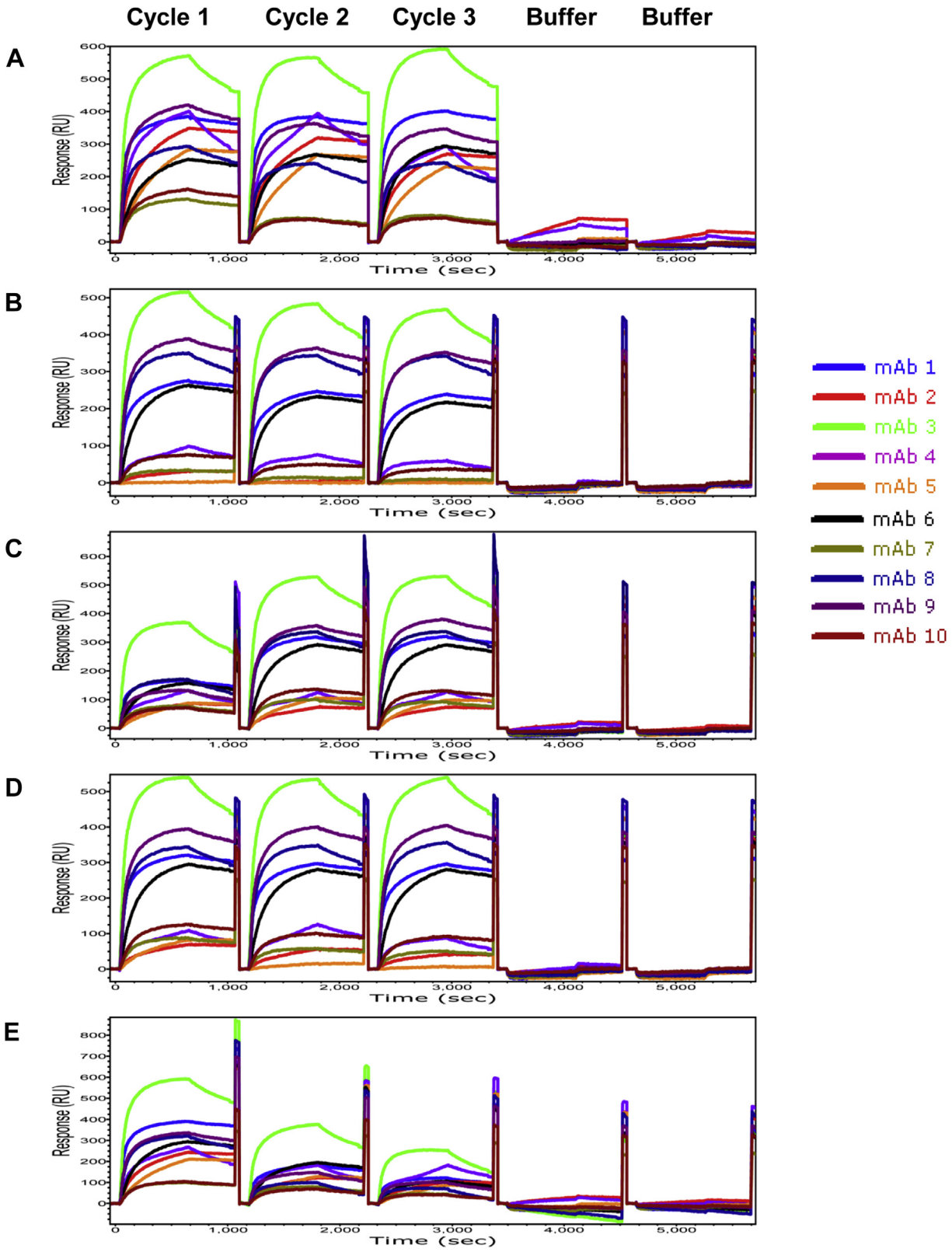

Fig. 3. Optimization of amine-coupled antibody surface regeneration in the IBIS MX96 using $MgCl_2$ (A), 1/500 H_3PO_4 (B), 10 mM glycine-HCl, pH 2.5 (C), 10 mM glycine-HCl, pH 2.0 (D), and 10 mM glycine-HCl, pH 1.5 (E). Each condition was assessed with 3 binding-regeneration cycles followed by 2 blank buffer injection cycles. Uniquely colored sensorgrams represent the mAbs indicated in the legend.

Although inconsistencies were observed in both antibody capture formats, the results of the Fc-captured antibody arrays were more inconsistent than those of the amine-coupled antibody arrays.

Surface regeneration

To enable multiple binding cycle measurements within the

Table 1
Preservation of amine-coupled antibody surface activities in the IBIS MX96 after regeneration. The percentages were calculated based on the binding signals generated after exposure to human PCSK9 following the third regeneration cycle in comparison to the initial binding signal prior to regeneration.

	$MgCl_2$	1/500 H_3PO_4	Glycine pH 2.5	Glycine pH 2.0	Glycine pH 1.5
mAb 1	100%	80%	>100%[a]	100%	30%
mAb 2	60%	0%	100%	0%	50%
mAb 3	100%	80%	>100%[a]	80%	50%
mAb 4	70%	80%	100%	80%	60%
mAb 5	90%	0%	100%	0%	50%
mAb 6	100%	80%	>100%[a]	90%	40%
mAb 7	50%	10%	100%	80%	40%
mAb 8	80%	100%	>100%[a]	100%	20%
mAb 9	70%	90%	>100%[a]	100%	30%
mAb 10	50%	50%	>100%[a]	80%	50%

[a] Incomplete regeneration.

same experiment, the protein A/G surfaces in the Biacore T100 and ProteOn XPR36 and the AHC sensor tips in the Octet RED384 were regenerated with a standard acidic solution (10 mM Glycine HCl [pH 1.5]). This regeneration condition successfully removed antibody-antigen complexes from the surface and returned the response signals to baseline. The use of both capturing reagents generated consistent mAb surface densities throughout the study (data not shown). The total number of binding-regeneration cycles was 60 in the Biacore T100 and 5 in the ProteOn XPR36 and Octet RED384. In the single-cycle kinetics experiment in the IBIS MX96, the antigen-bound antibody array captured by Protein A/G was not regenerated between each antigen injection.

To enable multi-cycle kinetic measurements using the IBIS MX96, the mAbs were directly immobilized onto the sensor through amine coupling, and the mAb surfaces were regenerated between antigen binding cycles. To identify regeneration conditions that would allow for complete antigen removal without affecting the antibody activity, an experiment was performed using different regeneration solutions. Fig. 3 shows the recorded binding response profiles of each mAb after one, two, and three regeneration cycles with the indicated regeneration solutions. An increase in subsequent antigen binding signals indicated incomplete antigen removal, whereas a decrease in subsequent antigen binding or blank injection signals indicated antibody surface deactivation. The results, which are summarized in Table 1, indicated that while none of the regeneration solutions succeeded in preserving 100% antibody activity for all of the mAbs, the glycine pH 2.0 solution worked the best among all the regeneration solutions as 8 of the 10 mAbs maintained >80% activity towards the antigen. The ranking is followed by 1/500 H_3PO_4 and 3 M $MgCl_2$ solutions, in which >80% binding activities were maintained in 6 and 5 of the 10 mAbs, respectively. Glycine pH 2.5 did not appear to remove all of the bound antigen, whereas glycine pH 1.5 caused substantial deactivation of the antibodies. Although glycine pH 2.0 was the preferred solution, two of the antibodies (mAb 2 and mAb 5) were completely deactivated after exposure to this solution. Thus, we decided to use two regeneration conditions. Glycine pH 2.5 was used to regenerate mAbs 2 and 5, while glycine pH 2.0 was used for the remaining mAbs.

Fig. 4 shows the comparison of the sensorgrams generated from the single- and multi-cycle kinetic experiments using the IBIS MX96. In the multi-cycle kinetic experiment, which included a regeneration step, the baseline returned to zero between each of the antigen binding steps, whereas in the single-cycle kinetic experiment, the baselines increased due to the absence of regeneration steps.

Ligand surface activity

Fig. 5 shows graphs of the mAb capture levels plotted against the R_{max} values obtained from the fitted binding curves. The plots containing the Biacore T100-, ProteOn XPR36-, or Octet RED384-generated data showed nearly linear correlations between the mAb capture levels (R_L) and the experimental R_{max} values, as illustrated by the high R^2 values (close to 1). Using these linear correlations, the activity of the ligand surface can be calculated from the slope (R_{max}/R_L), obtained from the linear regression fit, and compared to the molecular weight ratio of the analyte and the ligand. In this case, the molecular weight of human PCSK9 is 72.8 kDa and the molecular weight of the mAb is 75 kDa per analyte binding site, resulting in a mass ratio of 0.97. Once the slopes were obtained, the activity of each of the 10 mAbs was calculated (see Table 1 in Ref. [20]). In contrast to the positively correlated data generated from the Biacore, ProteOn, and Octet biosensors, the data from both the multi-cycle and single-cycle kinetic experiments using the IBIS MX96 generated R^2 values that were <0.5. In both cases, the mAb surface activities were calculated by analyzing the experimental R_{max}/theoretical R_{max} ratios as described in the Materials and Methods. Fig. 5F shows the calculated binding activities of the mAb surfaces across the biosensor platforms. While the activities associated with most of the systems were consistent, an ~10-fold lower activity was observed for the amine-coupled mAb surfaces associated with the IBIS MX96, possibly due to antibody inactivation or the generation of antibody orientations that were not conducive to antigen binding.

Background and blank subtraction

Prior to performing kinetic analysis on the binding curves, the background signals were examined to ensure there was no non-specific binding of the antigen to the reference surfaces. These reference surfaces refer to those of non-active flow cell (Biacore T100), inter-spots on the array (ProteOn XPR36 and IBIS MX96), and AHC sensor tips (Octet RED384) that were immobilized with capture reagent without any ligand present. In IBIS MX96, the reference surfaces are those unmodified inter-spot regions (see Fig. 2, *left panels*) where neither capture reagent nor ligand was spotted. In addition to background inspection, the blank signals from buffer injection over the active ligand surfaces were also examined to ensure there was no significant leaching of the ligand from the sensor surface throughout the entire binding event. Inclusion of both background and blank signals in data processing also allowed for the monitoring/correction of buffer bulk effect and systematic drift over time. Fig. 6 shows examples of the raw data collected on both active and reference surfaces in each of the four instruments. In all cases, there was no interaction of the antigen (up to 100 nM) to the reference surfaces on the sensor chips during the association phase (flat line also observed in AHC sensor tips dipped directly into antigen-containing wells, data not shown), validating that the

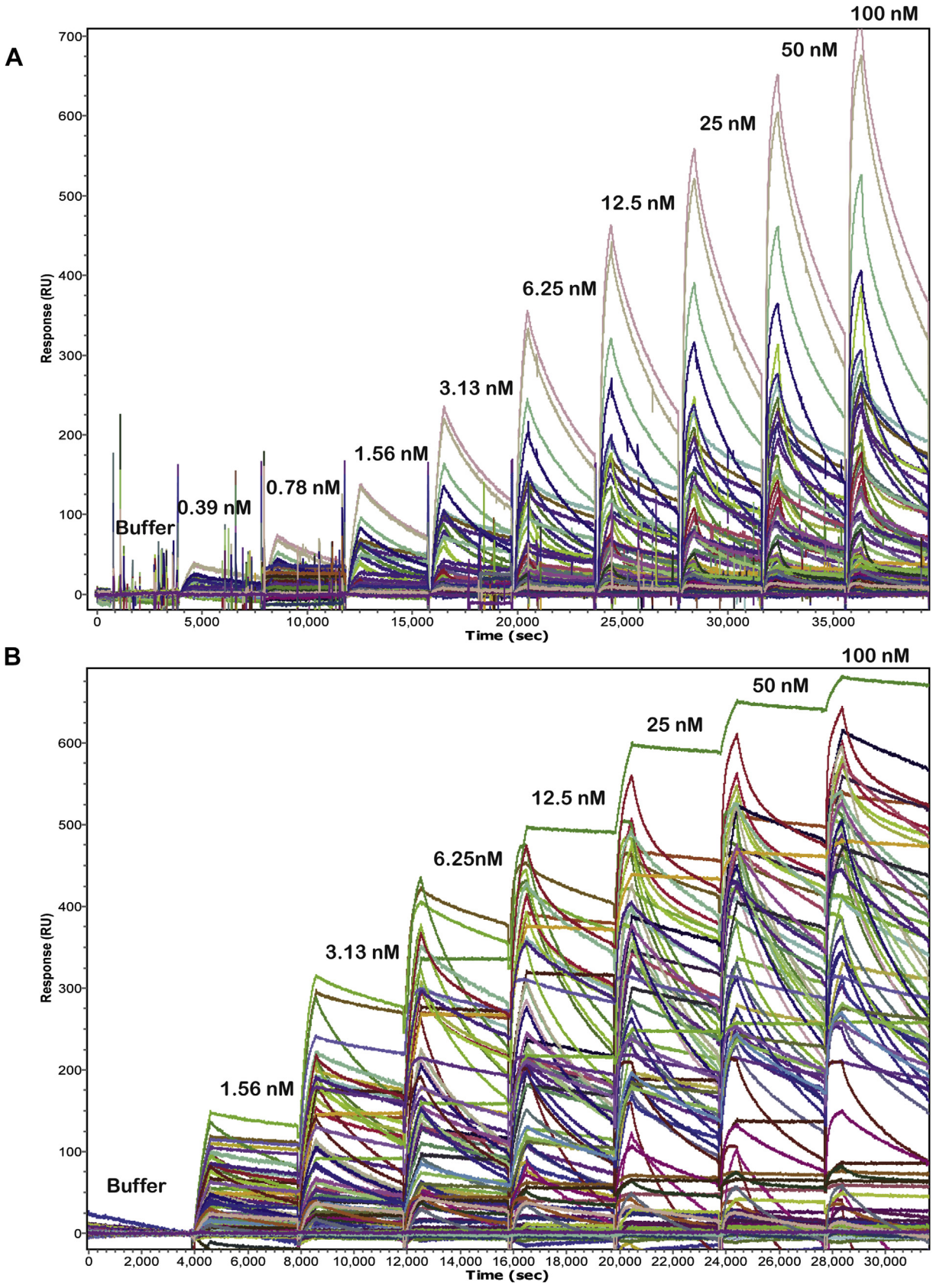

Fig. 4. MX96 binding sensorgram overlays from multi-cycle kinetic (A) and single-cycle kinetic (B) measurements. The antigen was injected at increasing concentrations (noted above each injection) across the 10 × 8 antibody array created from the CFM. Regeneration was performed between antigen injections in (A), but was not performed during the sequential antigen injections in (B).

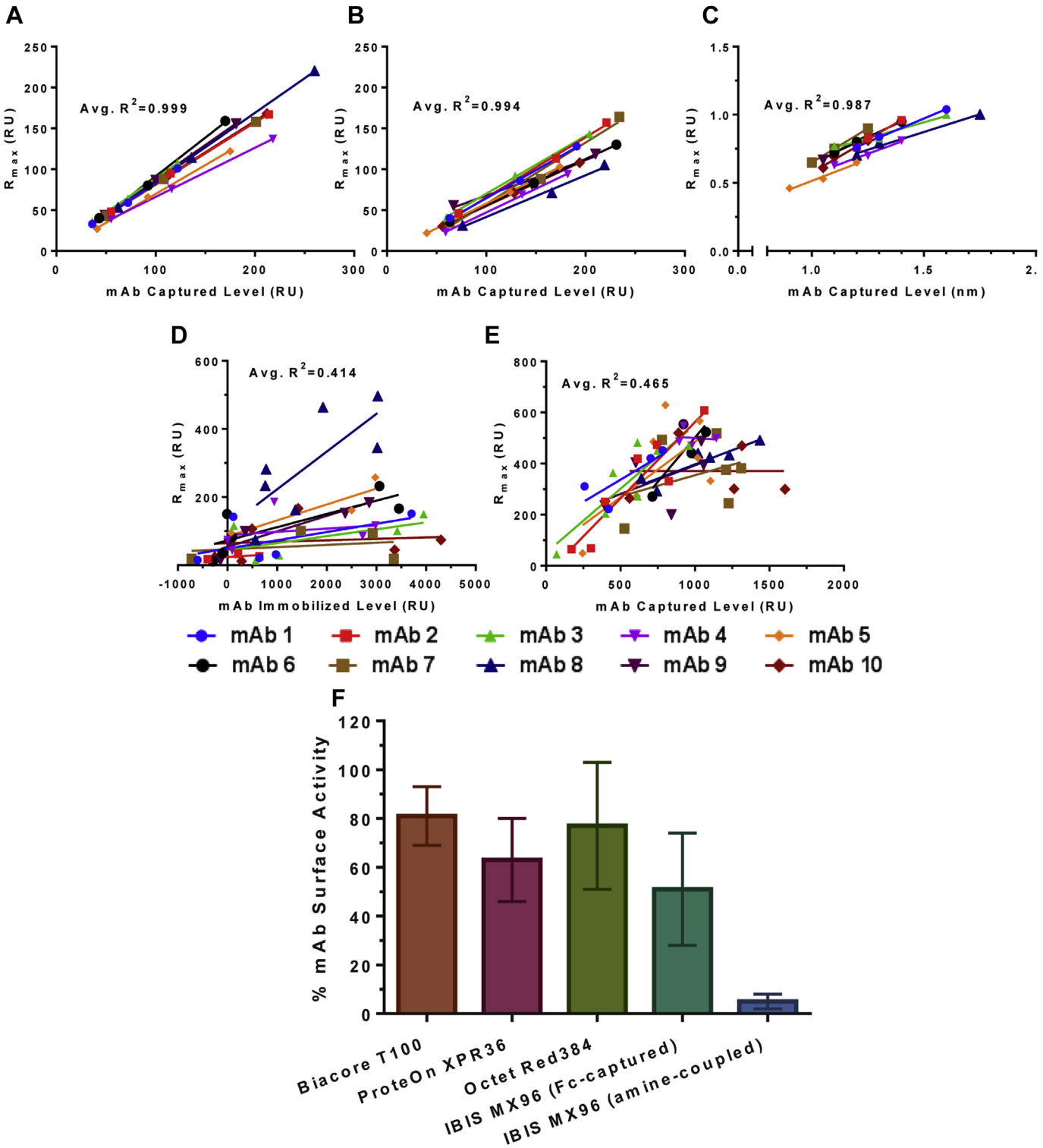

Fig. 5. Correlation of experimental R_{max} and antibody surface levels in the Biacore T100 (A), ProteOn XPR36 (B), Octet RED384 (C), IBIS MX96, amine-coupled (D), and IBIS MX96, Fc-captured (E). Each mAb is represented according to the legend. The R_{max} was obtained by fitting the binding curves using the 1:1 Langmuir kinetic model. The reported R^2 values (*inserts*) were generated by linear regression fitting of the plots. The mean activities of the mAb surfaces and their standard deviations (*error bars*) are shown in (F).

binding responses were highly specific to the antigen. As for the systematic drift, the maximal drift signal was observed to be ~10 RU in Biacore T100 (Fig. 6A, *right panels*), ~30 RU in ProteOn XPR 36 (Fig. 6B, *right panel*), ~0.15 nm in Octet RED384 (Fig. 6C, *right panel*), ~10 RU on the amine-coupled surface in IBIS MX96 (Fig. 6D, *left panel*), and ~20 RU on the protein A/G surface in IBIS MX96 (Fig. 6D, *left panel*). While the drifts in Octet RED384 and ProteOn XPR36 (the 100 nM curve) appeared to increase gradually with time in the dissociation phase, those of Biacore T100 and IBIS MX96 were relatively stable with fluctuations scattering along the baseline. To

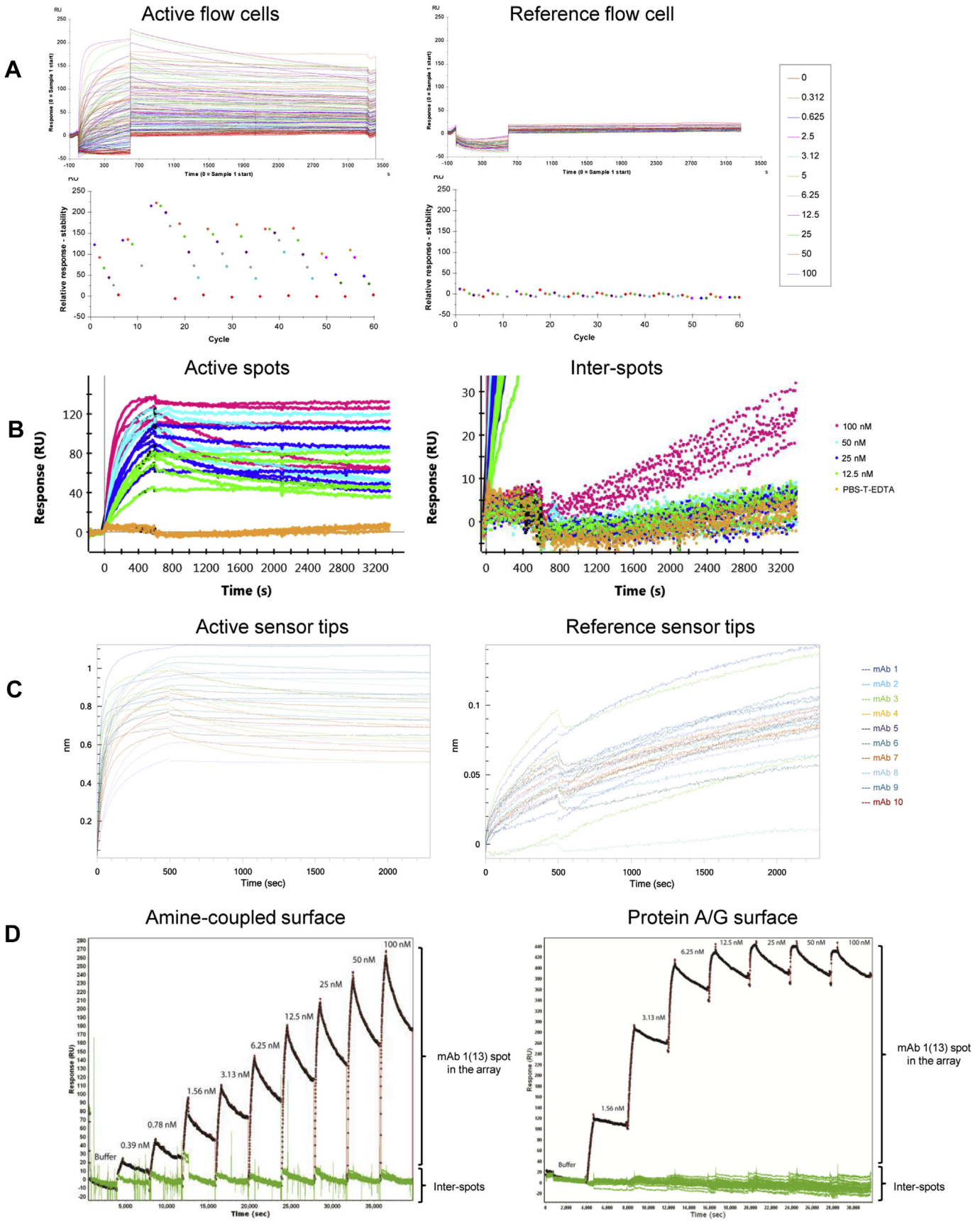

Fig. 6. Comparison of antigen binding and background/blank signals. Biacore T100 (A): antigen binding profiles (*top left panel*) and response signals (*bottom left panel*) over active flow cells 2–4, antigen binding profiles (*top right panel*) and response signals (*bottom right panel*) over reference flow cell 1. ProteOn XPR36 (B): antigen binding profiles on active channel L1 (*left panel*) and antigen binding profiles on reference inter-spots surrounding L1 (*right panel*). Octet RED384 (C): raw data from antibody-coated sensor tips dipped into individual sample wells containing 100 nM antigen (*left panel*) and antibody-coated sensor tips dipped into individual samples wells containing 1xKB running buffer (*right panel*). IBIS MX96 (D): raw data from mAb 1 on the amine-coupled (*left panel*) and protein A/G array surfaces (*right panel*), signals from the antibody spot are colored in black whereas that of inter-spots are colored in green. The sensorgrams shown are the un-processed raw data recorded in real-time from each of the instruments.

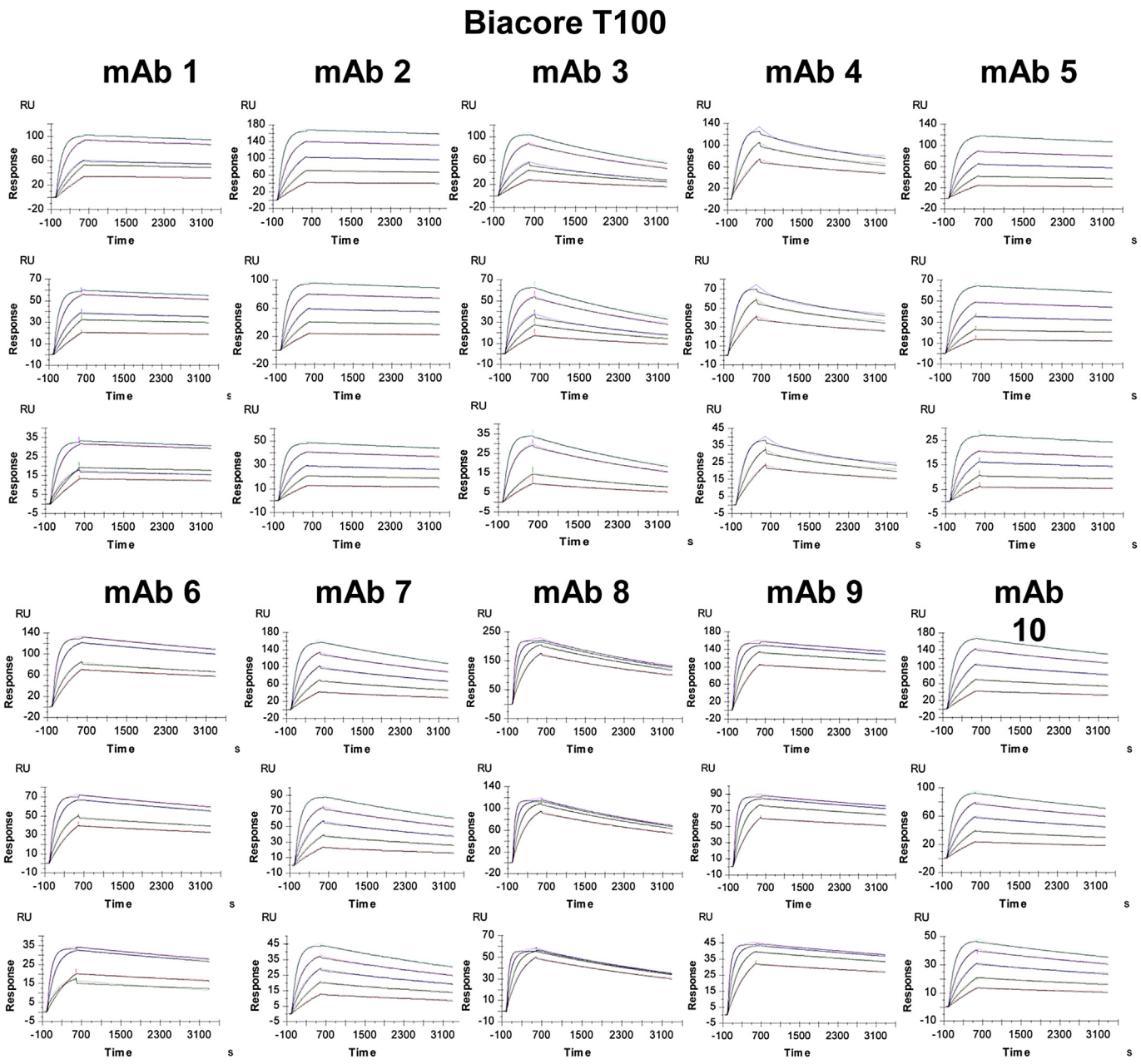

Fig. 7. Antigen binding profiles of the captured antibodies and 1:1 kinetic model fit overlays. The binding profiles were evaluated over high- (*top* panels), medium- (*middle* panels), and low- (*bottom* panels) density surfaces in the Biacore T100. The antibody ID is noted right above the corresponding sensorgrams. The colored lines represent the recorded binding response signals at different antigen concentrations, and the overlaid black lines represent the fitted curves.

correct for these inherent systematic artifacts, these drift signals were subtracted from the active sensorgrams to obtain the accurate binding profiles prior to the kinetic analysis.

Binding profiles and kinetic analysis

Figs. 7–10 show all of the processed data that were generated using the four biosensor platforms, grouped by antibody ID and sub-grouped by surface densities. On average, five antigen concentrations were used to provide evenly spaced binding curves containing both low and high responses that represented 10–90% ligand saturation. For comparison purposes, both the association (10 min) and dissociation (45 min) times were kept constant across the experiments; however, the experiments performed using Octet RED384 required shorter times (500 s association and 30 min dissociation) due to sample evaporation over time. Relatively long dissociation times were used to ensure the capture of signal decay for mAbs that exhibited slow off-rates. Visual comparison of the sensorgrams generated by the different instruments shows that while a majority of the binding curves contained sufficient signal decay for accurate off-rate analysis, upward drift during the dissociation phase was observed in some of the datasets generated by the Octet RED384 (e.g. mAb 2, mAb 5, and mAb 9; Fig. 9), resulting in higher end responses.

Overall, the binding profiles of the antibodies were similar across the instruments. High reproducibility was also observed in the binding data generated at varying surface densities using the Biacore T100, ProteOn XPR36, and Octet RED384. In contrast, the

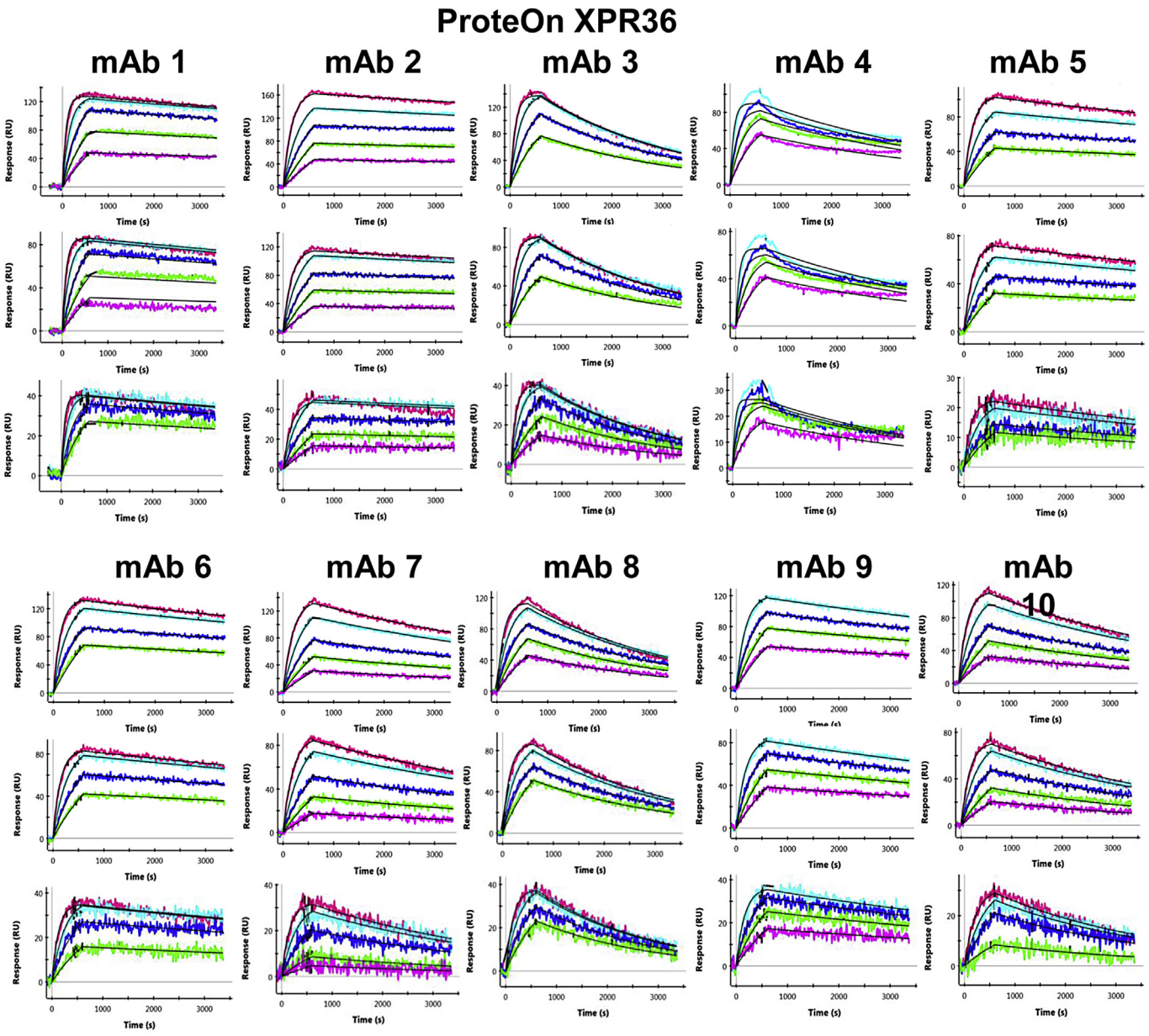

Fig. 8. Antigen binding profiles of the captured antibodies and 1:1 kinetic model fit overlays. The binding profiles were evaluated over high- (*top* panels), medium- (*middle* panels), and low- (*bottom* panels) density surfaces in the ProteOn XPR36. The antibody ID is noted right above the corresponding sensorgrams. The colored lines represent the recorded binding response signals at different antigen concentrations, and the overlaid black lines represent the fitted curves.

reproducibility was suboptimal in the IBIS MX96-generated data, in which 71% of the Fc-captured and 61% of the amine-coupled spots displayed acceptable binding signals for kinetic analysis, respectively. These values were determined based on the combination of three criteria assessed during the visual inspection of the raw data: 1. Insufficient binding signal of generally <10 RU, such as mAb 1 sensorgram (1) in both Fig. 10A and B where no binding was detected; 2. Spikes in the binding response curves, such as mAb 3 sensorgram (63) in Fig. 10A where a significant amount of spikes were introduced in the dissociation curve; and 3. Deviation of the binding profile compared to others within the same antibody, such as mAb 8 sensorgram (93) in Fig. 10B where the dissociation curve fell below 0 RU. With regard to the quality of the kinetic fits, visual inspection of the curves shows that most of the datasets returned an overlay of the response data with the model fit, indicating that the antibody-antigen interactions fit well to the chosen 1:1 kinetic model. However, mAb 4 appeared to display biphasic behavior that was observed on all four instruments. A low-quality fit of the response data was accompanied by a relatively high Chi^2 (or X^2) value (see Tables 2 and 3 in Ref. [20]). Taken together, these observations suggested that the antigen binding of mAb 4 is more complicated than that described by the simple 1:1 model.

To evaluate the variability of datasets generated within the same instrument, we compared kinetic rate constants generated using different antibody densities. Fig. 11 shows plots of k_a, k_d, and K_D at different mAb surface densities. Strong linearity was observed for all of the mAb rate constants generated using the Biacore T100 and ProteOn XPR36, indicating high reproducibility across the multiple surface densities. However, the rate constants generated by the Octet RED384 were less linear, possibly due to fluctuations in some of the off-rates. The rate constants generated by the IBIS MX96 were also less linear, possibly due to fluctuations in surface

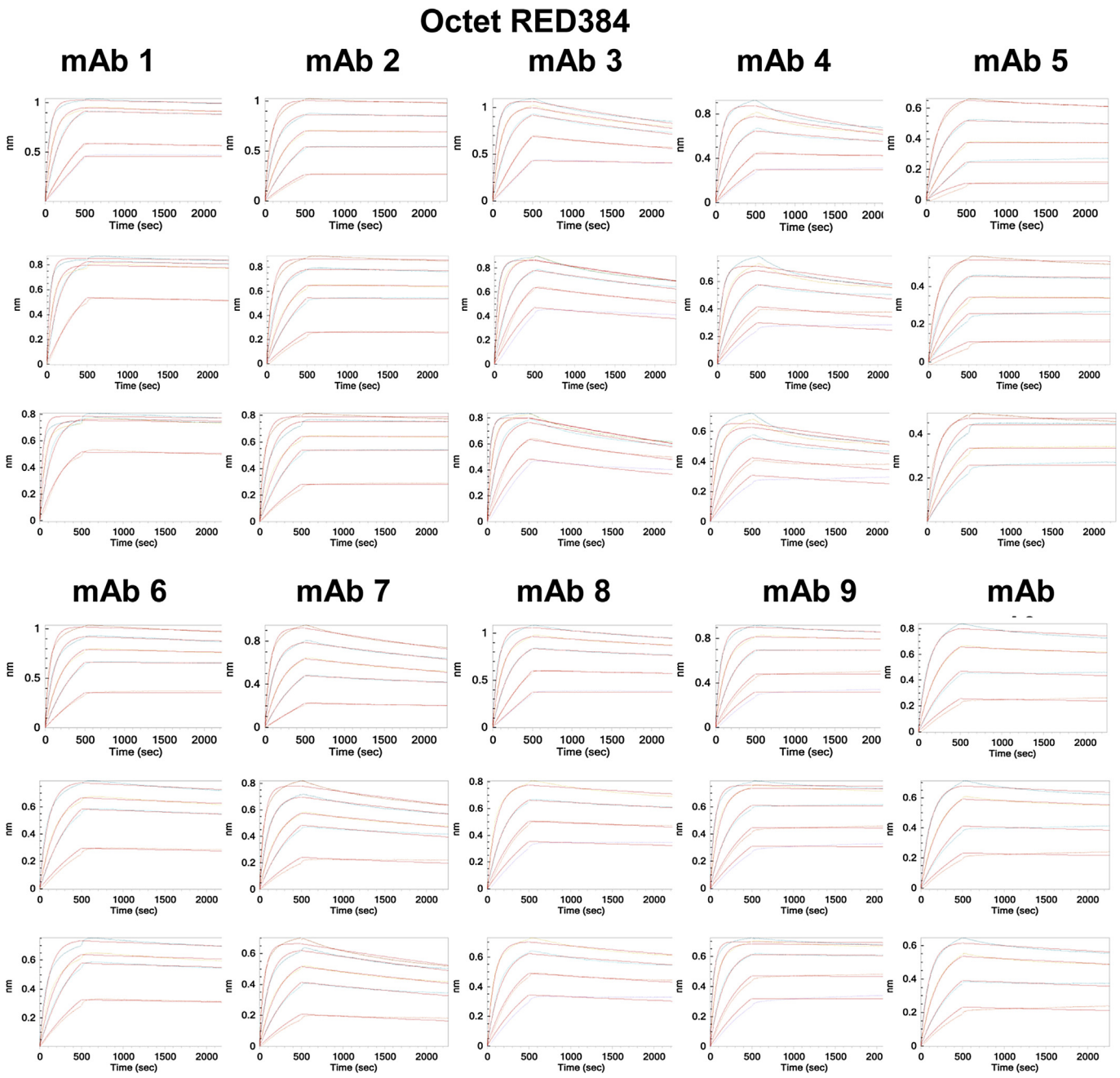

Fig. 9. Antigen binding profiles of the captured antibodies and 1:1 kinetic model fit overlays. The binding profiles were evaluated over high- (*top* panels), medium- (*middle* panels), and low- (*bottom* panels) density surfaces in the Octet RED384. The antibody ID is noted right above the corresponding sensorgrams. The colored lines represent the recorded binding response signals at different antigen concentrations, and the overlaid red lines represent the fitted curves.

heterogeneities. Statistical analysis of the analyzed K_D values observed across the multiple surfaces of the biosensors revealed the following deviations: Biacore T100: 6 (±6)%; ProteOn XPR36: 13 (±6)%; Octet RED384: 21 (±19)%; IBIS MX96, Fc-captured mAbs: 19 (±11)%; and IBIS MX96, amine-coupled mAbs: 28 (±13)%.

Distribution and comparison of binding kinetics

Fig. 12 provides a visual summary of the distribution of the kinetic rate constants generated by the different biosensors (see Table 4 in Ref. [20]). The affinities of the ten mAbs were all between 0.01 and 10 nM, with the majority between 0.1 and 1 nM. Both the association and dissociation rate constants spanned 1000-fold ranges. Table 2 lists the calculated affinities and rate constants of each of the ten mAbs, along with their standard deviations. Even though the rate constants associated with each of the antibodies varied across the instruments, their rank order remained mostly the same with two exceptions (Fig. 13). First, the k_a rank order of mAb 9 is lower than that of mAb 8 in ProteOn XPR36 (Fig. 13A, *green line*); and second, the k_d rank order of mAb 8 is lower than that of mAb 7 in Octet RED384 (Fig. 13B, *red line*). Additionally, the k_d values generated by the Octet RED384 (*red line*) were consistently lower than those from the other instruments. Likewise, the k_a values from the single-kinetic analysis in the IBIS MX96 (*orange line*) was lower in comparison to the others. To assess the general correlation propensity of the reported rate constants among the

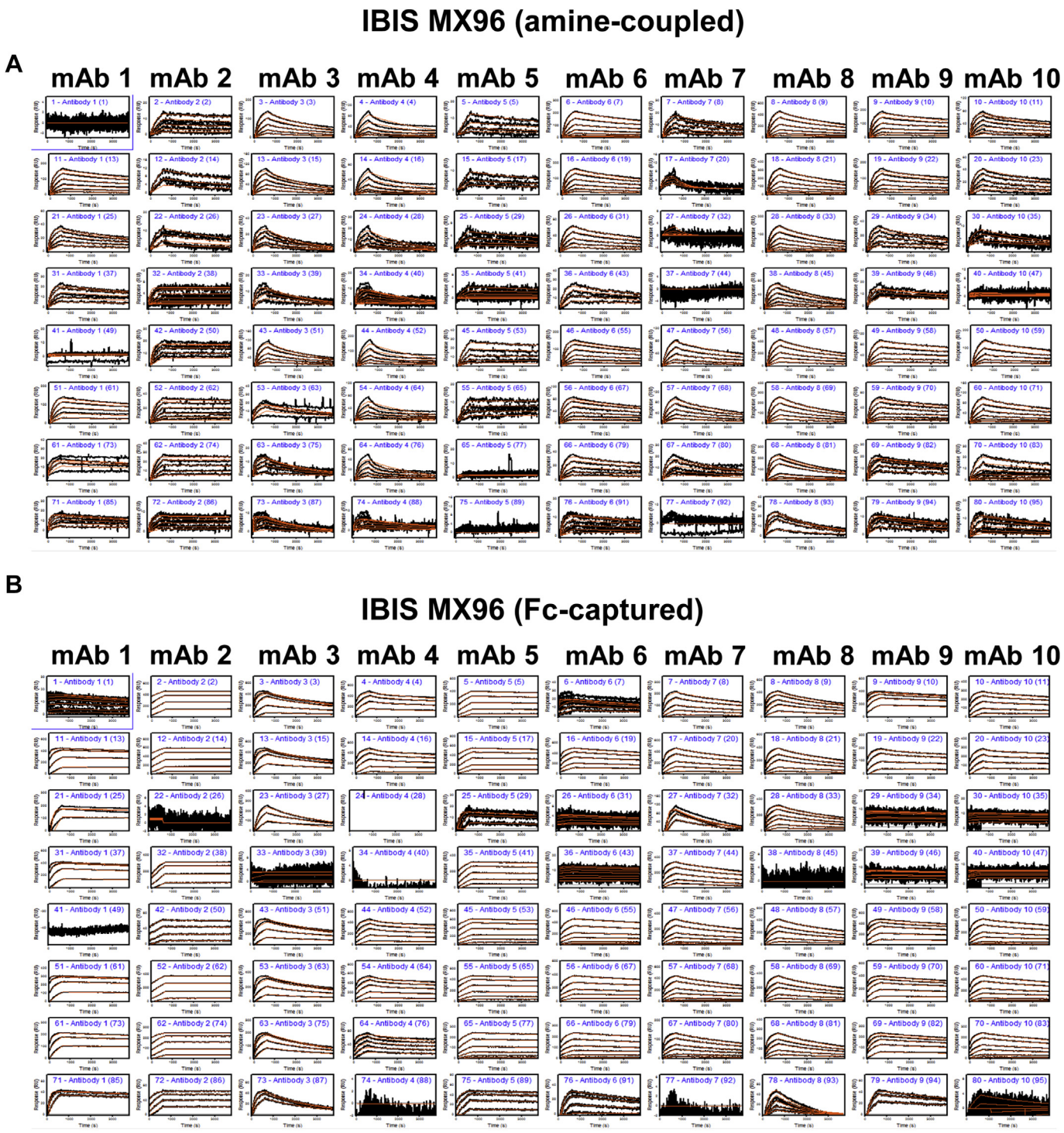

Fig. 10. Tiled view of the antigen binding profiles of the amine-coupled (A) and Fc-captured (B) antibodies in the 10 × 8 antibody array surfaces in the IBIS MX96. The antibody ID is noted right above the corresponding sensorgrams. Each mAb is accompanied by 8 vertical panels that follow the array plate map in Fig. 2. The black lines represent the recorded binding response signals, and the overlaid red lines represent the fitted curves.

instruments, statistical correlation analysis was performed. The results in Table 3 demonstrated that despite the two aforementioned exceptions, the kinetic rate and equilibrium binding constants were positively correlated across the instruments. In general, the individual rate constants determined on the instruments showed strong correlation when analyzed in a pairwise manner. One exception was the Octet RED384 – ProteOn XPR36 pair, which exhibited only moderate correlation strength in comparison to the others. Notably, the calculated affinities (K_D) showed slightly weaker correlations than those of the individual rate constants.

Discussion

This study was conducted to provide data-driven recommendations for the use of the four biosensor platforms by assessing their ability to provide quality kinetic data. Unlike previous

Table 2
Kinetic rates and equilibrium binding constants and their standard deviations determined from the four biosensor platforms.

	k_a (M^{-1} s^{-1})	k_a (% CV)	k_d (s^{-1})	k_d (% CV)	K_D (nM)	K_D (% CV)
mAb 1	11.7 (7.8) × 10^5	67	4.89 (4.18) × 10^{-5}	86	0.052 (0.05)	92
mAb 2	1.53 (0.28) × 10^5	19	1.30 (1.54) × 10^{-5}	118	0.092 (0.12)	128
mAb 3	11.4 (8.3) × 10^5	72	27.6 (11.0) × 10^{-5}	40	0.333 (0.20)	61
mAb 4	3.61 (1.6) × 10^5	45	20.1 (12.3) × 10^{-5}	61	0.659 (0.54)	83
mAb 5	0.59 (0.21) × 10^5	35	3.46 (2.50) × 10^{-5}	72	0.663 (0.46)	70
mAb 6	1.19 (0.78) × 10^5	65	7.21 (3.83) × 10^{-5}	53	0.894 (0.64)	72
mAb 7	1.29 (0.53) × 10^5	41	16.4 (5.63) × 10^{-5}	34	1.57 (1.02)	65
mAb 8	4.02 (2.23) × 10^5	55	22.8 (10.7) × 10^{-5}	47	0.768 (0.68)	88
mAb 9	4.20 (2.13) × 10^5	51	6.67 (4.3) × 10^{-5}	64	0.197 (0.16)	82
mAb 10	1.20 (0.49) × 10^5	41	12.5 (7.64) × 10^{-5}	61	1.27 (0.80)	63
	Average k_a %CV	49	Average k_d %CV	64	Average K_D %CV	80

Table 3
Correlation of kinetic rates and equilibrium binding constants among the biosensor platforms. Positive correlation coefficients (r) indicate positive correlations and r values close to 1 indicate stronger correlations. The correlation strength is defined as follows: very strong (0.8–1.0, dark green), strong (0.60–0.79, light green), and moderate (0.40–0.59, yellow).

Correlation coefficient (r)	k_a correlation					k_d correlation					K_D correlation				
	Biacore T100	ProteOn XPR36	Octet RED384	IBIS MX96 (amine-coupled)	IBIS MX96 (Fc-capture)	Biacore T100	ProteOn XPR36	Octet RED384	IBIS MX96 (amine-coupled)	IBIS MX96 (Fc-capture)	Biacore T100	ProteOn XPR36	Octet RED384	IBIS MX96 (amine-coupled)	IBIS MX96 (Fc-capture)
Biacore T100	---	0.966****	0.821****	0.895****	0.962***	---	0.911****	0.927****	0.974****	0.864****	---	0.869****	0.706**	0.858****	0.833****
ProteOn XPR36	0.966****	---	0.775***	0.858****	0.932***	0.911****	---	0.787***	0.860****	0.886****	0.869****	---	0.470*	0.776***	0.701**
Octet RED384	0.821****	0.775***	---	0.862****	0.792***	0.927****	0.787***	---	0.921****	0.858****	0.706**	0.470*	---	0.722**	0.841****
IBIS MX96 (amine-coupled)	0.895****	0.858****	0.862****	---	0.919***	0.974****	0.860****	0.921****	---	0.824****	0.858****	0.776***	0.722**	---	0.756**
IBIS MX96 (Fc-capture)	0.962****	0.932****	0.792***	0.919****	---	0.864***	0.886****	0.858****	0.824****	---	0.833****	0.701**	0.841****	0.756**	---

* P>0.05

** 0.01<P<0.05

*** 0.005<P<0.01

****P<0.005

benchmark studies that involved the analysis of only single antibody-antigen binding pairs, and recruited a large number of participants who used the same biosensor technology with the same assay format [8], or different biosensor technologies with variable assay formats [17], our study expanded the number of analyzed binding interactions (10 mAbs against the same antigen), while limiting external factors that could influence data variability. For example, we limited the number of hands-on researchers to two, performed the experiments on all four biosensor platforms simultaneously, and used the same high-quality reagents throughout the study.

Our results showed that the instruments with continuous flow fluidics (the Biacore T100, ProteOn XPR36, and IBIS MX96) provided high-quality data for resolving high-affinity interactions (0.1–1.0 nM) with slow dissociation rates. Upward drifts in the dissociation curves were observed in some of the datasets gathered from the Octet RED384 BLI platform that were likely due to sample evaporation over time in the microplate, which is a well-known primary limitation of the system. Re-binding of the antigen in each sample well was also a possibility, but according to the manufacturer, this can be minimized by the orbital agitation of the microplate at high speed. Nevertheless, these two potential limitations have presented uncertainties in analyzing high-affinity binding interactions of our antibodies as compared to the fluidic platforms. Further analysis showed that when the Octet RED384-generated rate constants were excluded from the global calculations, an ~20% improvement in both the average k_d and K_D standard deviations (from 64% to 47% and 80%–61%, respectively) was observed, while the k_a deviation remained the same, further supporting the notion that the Octet RED384's inherent limitation renders the analysis of slow dissociation profiles inaccurate.

We also found inconsistencies in the generation of the antibody array by the CFM in the IBIS MX96. For accurate kinetic measurements, the amount of ligand on the biosensor surface is a critical parameter that needs to be controlled to ensure that the binding responses are not disturbed by secondary factors such as mass

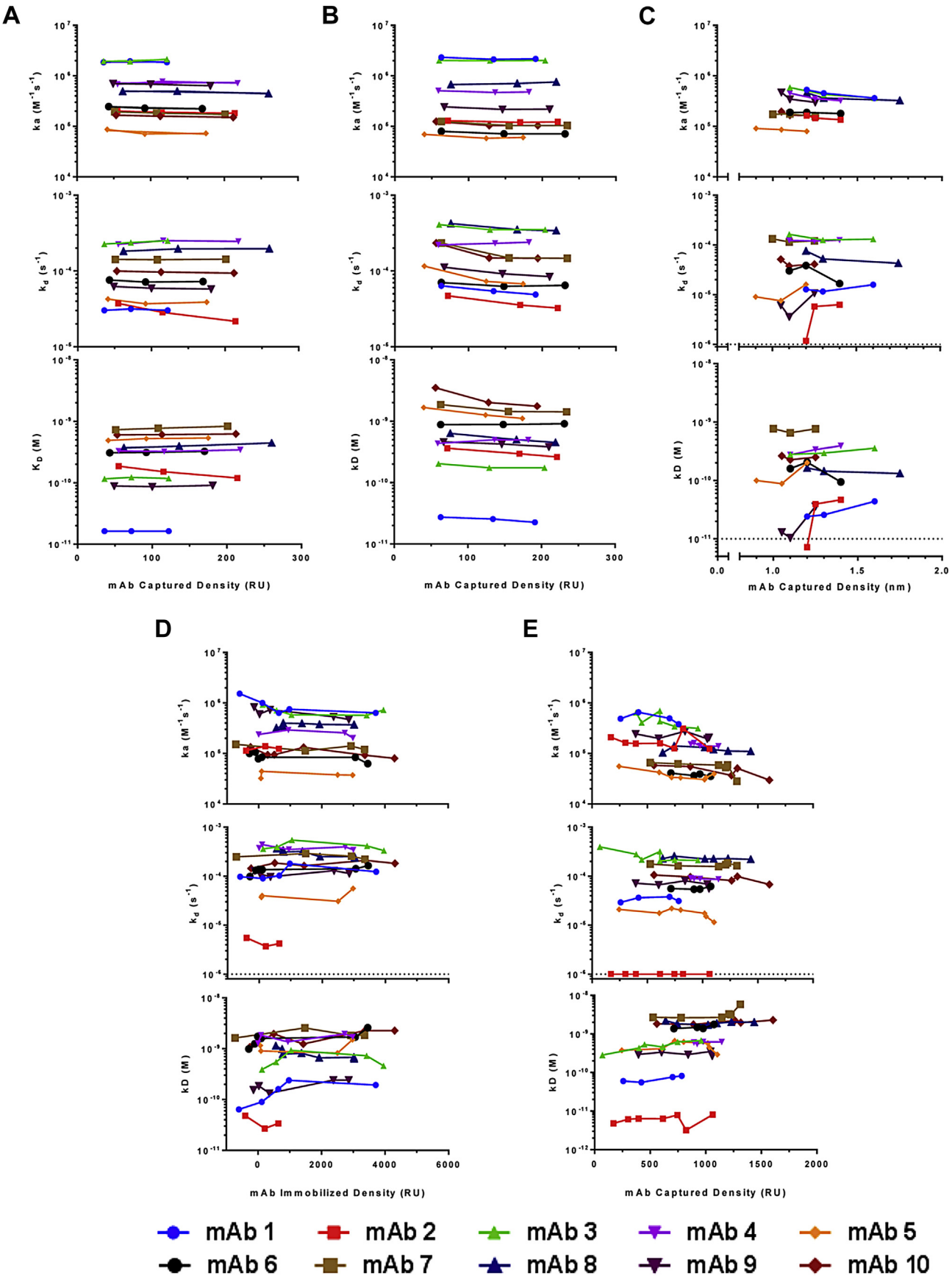

Fig. 11. Correlation of kinetic rate constants and antibody surface densities in the Biacore T100 (A), ProteOn XPR36 (B), Octet RED384 (C), IBIS MX96, amine-coupled (D), and IBIS MX96, Fc-captured (E). The k_a, k_d, and K_D calculated from the individual fitted curves are shown in the *top*, *middle*, and *bottom* sub-panels, respectively. The mAbs are identified in the legend.

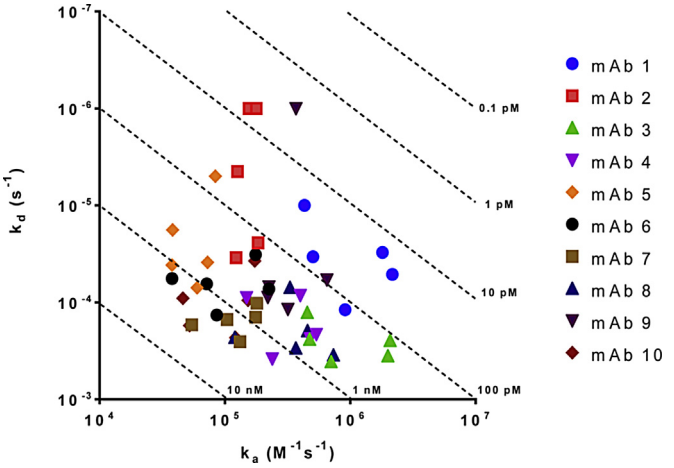

Fig. 12. Two-dimensional isoaffinity kinetic plot of rate constants grouped by antibody. The dashed diagonals depict the equilibrium binding constants and are shown to help with the visualization of the affinity distribution.

transfer or steric hindrance [21]. However, the lack of consistent ligand immobilization combined with inefficient array printing in this instrument, resulted in reduced data reproducibility. In addition, our observation that some of the binding response levels were relatively high suggested that we could not rule out the possibility of surface complications in the influence of rate constant accuracy. We also found that certain aspects of this system were suboptimal for the purpose of high-resolution kinetic constant determinations. For example, the separation of the CFM device from the MX96 detector was inconvenient for performing multi-cycle kinetic experiments. Not only did this setup require the ligands, in this case our 10 mAbs, to be directly immobilized onto the sensor surface through amine coupling, but it also required optimal regeneration conditions to be determined in advance, which had extended the total experimental time. Given the known issue of surface heterogeneity from the amine coupling and regeneration process to yield variable results, the low ligand activity and high K_D inconsistency associated with this setup were somewhat expected.

As an alternative approach, we adapted a single-cycle kinetics setup [22], which does not require regeneration, to the IBIS MX96. The elimination of surface regeneration also allowed us to incorporate the Fc-capture method into this experiment. Multiple studies have shown that the single-cycle kinetic approach yields results that are comparable to that of traditional approaches with added advantages in reagent and time savings [22–24]. Using this approach, we found that the calculated affinities and off-rates were consistent with those generated using the multi-cycle kinetic approach. In particular, excluding the K_D and k_d values generated from this approach from the global calculations had no effect on the standard deviations. However, the single-cycle kinetic-generated k_a values were lower than the values produced by the other biosensor systems in 6 of the 10 mAbs. Further analysis showed an ~10% improvement in the global k_a deviation (from 49% to 39%) when the single-cycle kinetics k_a value was excluded from the calculation. The decreased k_a was probably due to the depletion of ligand-binding sites along with increasing steric hindrance as the antibody-antigen complexes accumulated on the surface. Regardless, the mAb affinities were not significantly affected.

Overall, we found that the Biacore T100 generated the most consistent data, followed by the ProteOn XPR36, and the Octet RED384 and IBIS MX96, which generated comparable but lower quality data. However, the Biacore T100 platform also ranked lowest in sample throughput. This limitation was overcome by the other three platforms, which expanded the number of interactions

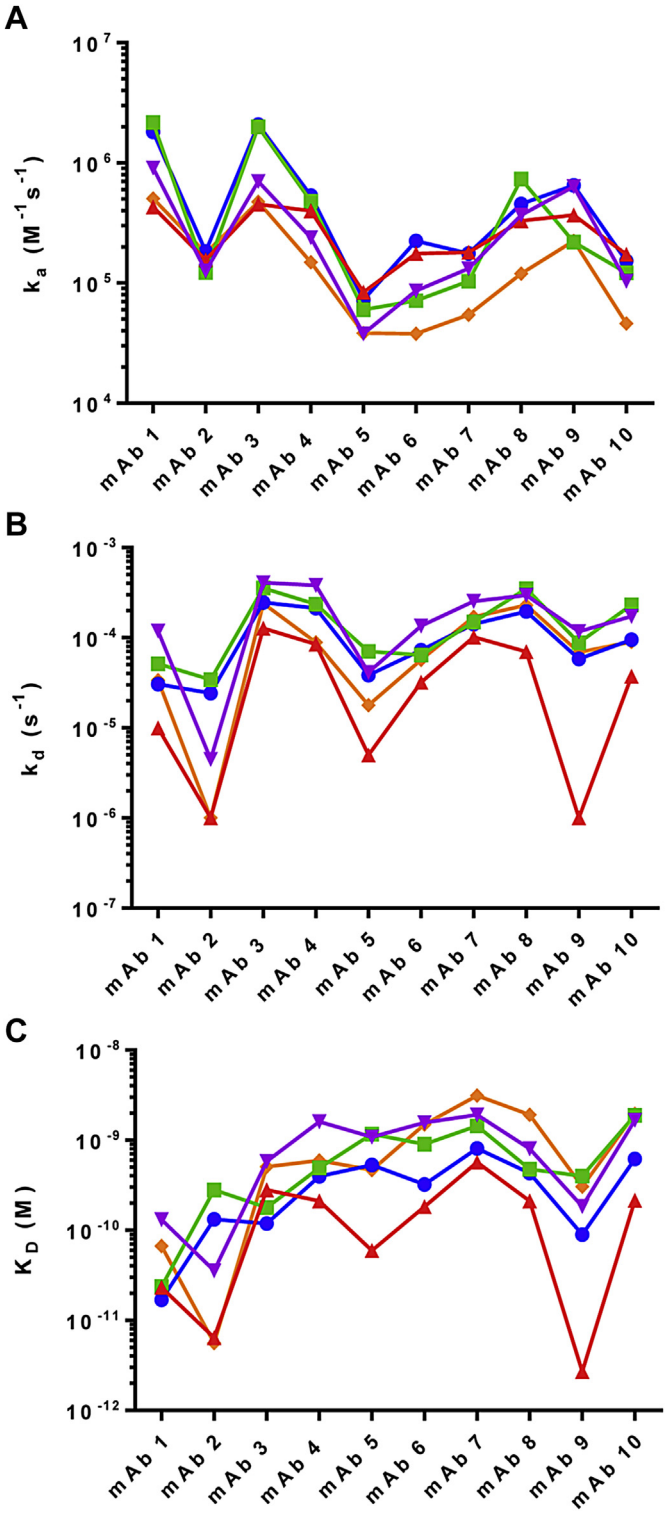

Fig. 13. Comparison of the kinetic rates and equilibrium binding constants generated by the biosensor platforms. The k_a, k_d, and K_D for each antibody, as calculated from Figs. 6–9, are shown in (A), (B), and (C), respectively. The instruments are represented as follows: Biacore T100 (blue), ProteOn XPR36 (green), Octet RED384 (red), IBIS MX96, amine-coupled (purple), and IBIS MX96, Fc-captured (orange).

measured in a single binding cycle to 36 (ProteOn XPR36), 16 (Octet RED384), and 96 (IBIS MX96). Since our experiments incorporated long dissociation times, there were no significant differences in the experimental times of these three platforms, and in all cases the

experiments were completed in one day. On the other hand, the Biacore T100 experiments required 3 days to complete, despite the walk-away automation in data acquisition after the setup. With respect to user hands-on time, a unique feature of the Octet platform is the availability of pre-coated sensors for immediate use, resulting in the reduction of preparation time by eliminating the need for ligand immobilization. On the other hand, the sensor chip initiation and pre-conditioning steps in the ProteOn XPR36 adds more hands-on time when compared to both Biacore and Octet platforms. Similarly, the microarray printing for the IBIS MX96 platform is also a relatively attentive and time-consuming procedure. Even though the preparation time can be offset by the analysis of ten mAbs simultaneously, we found that we benefited from inserting multiple mAb concentration spots on the array to counteract the printing inconsistency. With regard to the material consumption, the total amounts of samples consumed on each of the four biosensor platforms was roughly equivalent in our experiments which involved multiple ligand surfaces and analyte injections. Even though the Octet platform allows for the materials to be recovered, most of our samples had evaporated from the open microplate after the overnight run.

The ability of antibodies to bind their targets with high affinity and specificity has made them very attractive therapeutic modalities. However, characterizing high-affinity antibody-antigen interactions can be technically challenging when the instruments' detection limits are reached. Although the majority of the calculated rate constants fall below the typical uppermost association detection limit (1×10^7 in Biacore T100 [25], 3×10^6 in ProteOn XPR36 [26], 1×10^7 in Octet RED384 [27] and 5×10^6 in IBIS MX96 [28], in the unit of M^{-1} s^{-1}), as well as above the typical lowest dissociation detection limit (1×10^{-5} in Biacore T100 [25], 1×10^{-6} in ProteOn XPR36 [26], 1×10^{-6} in Octet RED384 [27] and 2×10^{-6} in IBIS MX96 [28], in the unit of s^{-1}) of respective systems according to the manufacturers' specifications, a number of them approach these limits with <5-fold differences (see Tables 5 in Ref. [20]). As the binding interactions approach these typical limits, it is instinctive for researchers to raise concern about the accuracy of the analyzed kinetic parameters. However, findings from our studies showed that working limits should be considered with caution as they also depend upon other important factors such as the inherent limitations of the systems and the experimental conditions. For example, although the described Biacore T100 dissociation limit is an order of magnitude higher than the others, the high quality data generated from our head-to-head comparison study suggested that the working limit was at the least comparable with the ProteOn XPR36, and better than both Octet RED384 and IBIS MX96. On the contrary, the aforementioned limitations in Octet RED384 presented challenges in producing accurate dissociation curves despite expectations for resolving slow off-rates based on its specifications. Similarly, the underlying limitation of the experimental designs involving amine-coupled and non-regenerative protein A/G surfaces in IBIS MX96 compromised the accuracy of the on-rates, regardless whether the instrument was capable of producing data within the expected limits.

Taking all the data obtained from the four biosensor platforms together, our calculations of the rate constants on these antibodies with sub-nanomolar antigen affinity revealed the following deviations: 49 (±17)% in k_a, 64 (±24)% in k_d, and 80 (±20)% in K_D. Even though our results indicated an expected trade-off between data accuracy/consistency and sample throughput, the rank order of the acquired kinetic rate constants was highly consistent across the instruments. Despite certain limitations in instrumentation that impacted data accuracy, these platforms generated binding data that fit the simple 1:1 molecular interaction model, and were capable of identifying those profiles that deviated from the model. Deviations in the kinetic binding data that we observed resulted from differences in the methodologies of the platforms. Each platform has its own advantages and disadvantages, the latter of which may or may not be tolerated, depending on the experimental goals of the researcher. For example, even though the Octet RED384 is limited in its ability to resolve slow dissociation interactions, it is highly flexible with regard to sensor choice and assay configuration, in addition to ease of operation. Although the throughput of the IBIS MX96 is orders of magnitude higher than that of the other biosensors, the robustness in its array printing requires substantial improvement to fully utilize its throughput advantage. Regardless, it is one of the few instruments (along with the Octet) that are equipped for effective combinatorial epitope binning analysis and has the potential to become an extremely versatile tool if its performance can be improved. With the discontinuation of the ProteOn XPR36 in the near future, it is unclear whether its high quality performance can be maintained given the unknown availability of future instrument support. Taken together, for studies that require sensitive and reliable detection, either Biacore T100 or ProteOn XPR36 is best suited. Whereas for studies in which speed is a critical factor and large number of samples (i.e. in the hundreds) are involved, either Octet RED384 or IBIS MX96 is preferred as both offer the throughput and efficiency needed for rapid data acquisition. For the purpose of candidate ranking, assuming the number of samples and the amount of materials are not limiting factors, any of these instruments may be used, as our results demonstrated that the obtained rate constants differentiated the antibodies comparably irrespective of which instrument was used.

In summary, our unbiased results may not only help new biosensor users determine the best instrument for their research purposes, thereby maximizing the value of their investment, but may also provide additional insights to current biosensor users regarding the systematic factors that influence data reliability, to enable the appropriate selection of biosensor instruments for their studies.

Author contributions

D.Y wrote the manuscript. D.Y. and A.J. performed the experiments and analyzed the data. H.W helped set up the Biacore T100 experiment. R.K. provided technical guidance, conceptual advice and oversight throughout the entire process. All authors discussed the results and implications and commented on the manuscript at all stages.

Acknowledgment

The authors would like to thank Noah Ditto and Adam Miles for technical assistance on the IBIS MX96, Tim Fenn for helpful discussions, and Sanjaya Singh for the conceptual guidance and critical reading of the manuscript.

References

[1] D.G. Myszka, Kinetic analysis of macromolecular interactions using surface plasmon resonance biosensors, Curr. Opin. Biotechnol. 8 (1997) 50–57, http://dx.doi.org/10.1016/S0958-1669(97)80157-7.
[2] J.M. McDonnell, Surface plasmon resonance: towards an understanding of the mechanisms of biological molecular recognition, Curr. Opin. Chem. Biol. 5 (2001) 572–577, http://dx.doi.org/10.1016/S1367-5931(00)00251-9.
[3] M.A. Cooper, Optical biosensors in drug discovery, Nat. Rev. Drug Discov. 1 (2002) 515–528, http://dx.doi.org/10.1038/nrd838.
[4] M.H. Van Regenmortel, D. Altschuh, J. Chatellier, L. Christensen, N. Rauffer-Bruyère, P. Richalet-Secordel, J. Witz, G. Zeder-Lutz, Measurement of antigen-antibody interactions with biosensors, J. Mol. Recognit. JMR 11 (1998) 163–167, http://dx.doi.org/10.1002/(SICI)1099-1352(199812)11:1/6<163::AID-JMR414>3.0.CO;2-U.
[5] D.G. Myszka, Kinetic, equilibrium, and thermodynamic analysis of

macromolecular interactions with BIACORE, in: B.-M (Ed.), Enzymology, Academic Press, 2000, pp. 325–340. http://www.sciencedirect.com/science/article/pii/S0076687900233727 (accessed 02.02.16).
[6] S.N. Davidoff, N.T. Ditto, A.E. Brooks, J. Eckman, B.D. Brooks, Surface plasmon resonance for therapeutic antibody characterization, in: Y. Fang (Ed.), Label-free Biosens. Methods Drug Discov., Springer New York, New York, NY, 2015, pp. 35–76. http://link.springer.com/10.1007/978-1-4939-2617-6_3 (accessed 02.02.16).
[7] G.A. Canziani, S. Klakamp, D.G. Myszka, Kinetic screening of antibodies from crude hybridoma samples using Biacore, Anal. Biochem. 325 (2004) 301–307.
[8] P.S. Katsamba, I. Navratilova, M. Calderon-Cacia, L. Fan, K. Thornton, M. Zhu, T.V. Bos, C. Forte, D. Friend, I. Laird-Offringa, G. Tavares, J. Whatley, E. Shi, A. Widom, K.C. Lindquist, S. Klakamp, A. Drake, D. Bohmann, M. Roell, L. Rose, J. Dorocke, B. Roth, B. Luginbühl, D.G. Myszka, Kinetic analysis of a high-affinity antibody/antigen interaction performed by multiple Biacore users, Anal. Biochem. 352 (2006) 208–221, http://dx.doi.org/10.1016/j.ab.2006.01.034.
[9] Y.N. Abdiche, A. Miles, J. Eckman, D. Foletti, T.J. Van Blarcom, Y.A. Yeung, J. Pons, A. Rajpal, High-throughput epitope binning assays on label-free array-based biosensors can yield exquisite epitope discrimination that facilitates the selection of monoclonal antibodies with functional activity, PLoS One 9 (2014) e92451, http://dx.doi.org/10.1371/journal.pone.0092451.
[10] J.P. Davda, R.J. Hansen, Properties of a general PK/PD model of antibody-ligand interactions for therapeutic antibodies that bind to soluble endogenous targets, mAbs 2 (2010) 576–588, http://dx.doi.org/10.4161/mabs.2.5.12833.
[11] A.M. Scott, J.D. Wolchok, L.J. Old, Antibody therapy of cancer, Nat. Rev. Cancer 12 (2012) 278–287, http://dx.doi.org/10.1038/nrc3236.
[12] C. Spiess, Q. Zhai, P.J. Carter, Alternative molecular formats and therapeutic applications for bispecific antibodies, Mol. Immunol. 67 (2015) 95–106, http://dx.doi.org/10.1016/j.molimm.2015.01.003.
[13] R.L. Rich, D.G. Myszka, Higher-throughput, label-free, real-time molecular interaction analysis, Anal. Biochem. 361 (2007) 1–6, http://dx.doi.org/10.1016/j.ab.2006.10.040.
[14] M.A. Eddings, A.R. Miles, J.W. Eckman, J. Kim, R.L. Rich, B.K. Gale, D.G. Myszka, Improved continuous-flow print head for micro-array deposition, Anal. Biochem. 382 (2008) 55–59, http://dx.doi.org/10.1016/j.ab.2008.07.031.
[15] J.B. Beusink, A.M.C. Lokate, G.A.J. Besselink, G.J.M. Pruijn, R.B.M. Schasfoort, Angle-scanning SPR imaging for detection of biomolecular interactions on microarrays, Biosens. Bioelectron. 23 (2008) 839–844, http://dx.doi.org/10.1016/j.bios.2007.08.025.
[16] J. Concepcion, K. Witte, C. Wartchow, S. Choo, D. Yao, H. Persson, J. Wei, P. Li, B. Heidecker, W. Ma, R. Varma, L.-S. Zhao, D. Perillat, G. Carricato, M. Recknor, K. Du, H. Ho, T. Ellis, J. Gamez, M. Howes, J. Phi-Wilson, S. Lockard, R. Zuk, H. Tan, Label-free detection of biomolecular interactions using BioLayer interferometry for kinetic characterization, Comb. Chem. High. Throughput Screen 12 (2009) 791–800.
[17] R.L. Rich, G.A. Papalia, P.J. Flynn, J. Furneisen, J. Quinn, J.S. Klein, P.S. Katsamba, M.B. Waddell, M. Scott, J. Thompson, J. Berlier, S. Corry, M. Baltzinger, G. Zeder-Lutz, A. Schoenemann, A. Clabbers, S. Wieckowski, M.M. Murphy, P. Page, T.E. Ryan, J. Duffner, T. Ganguly, J. Corbin, S. Gautam, G. Anderluh, A. Bavdek, D. Reichmann, S.P. Yadav, E. Hommema, E. Pol, A. Drake, S. Klakamp, T. Chapman, D. Kernaghan, K. Miller, J. Schuman, K. Lindquist, K. Herlihy, M.B. Murphy, R. Bohnsack, B. Andrien, P. Brandani, D. Terwey, R. Millican, R.J. Darling, L. Wang, Q. Carter, J. Dotzlaf, J. Lopez-Sagaseta, I. Campbell, P. Torreri, S. Hoos, P. England, Y. Liu, Y. Abdiche, D. Malashock, A. Pinkerton, M. Wong, E. Lafer, C. Hinck, K. Thompson, C.D. Primo, A. Joyce, J. Brooks, F. Torta, A.B. Bagge Hagel, J. Krarup, J. Pass, M. Ferreira, S. Shikov, M. Mikolajczyk, Y. Abe, G. Barbato, A.M. Giannetti, G. Krishnamoorthy, B. Beusink, D. Satpaev, T. Tsang, E. Fang, J. Partridge, S. Brohawn, J. Horn, O. Pritsch, G. Obal, S. Nilapwar, B. Busby, G. Gutierrez-Sanchez, R.D. Gupta, S. Canepa, K. Witte, Z. Nikolovska-Coleska, Y.H. Cho, R. D'Agata, K. Schlick, R. Calvert, E.M. Munoz, M.J. Hernaiz, T. Bravman, M. Dines, M.-H. Yang, A. Puskas, E. Boni, J. Li, M. Wear, A. Grinberg, J. Baardsnes, O. Dolezal, M. Gainey, H. Anderson, J. Peng, M. Lewis, P. Spies, Q. Trinh, S. Bibikov, J. Raymond, M. Yousef, V. Chandrasekaran, Y. Feng, A. Emerick, S. Mundodo, R. Guimaraes, K. McGirr, Y.-J. Li, H. Hughes, H. Mantz, R. Skrabana, M. Witmer, J. Ballard, L. Martin, P. Skladal, G. Korza, I. Laird-Offringa, C.S. Lee, A. Khadir, F. Podlaski, P. Neuner, J. Rothacker, A. Rafique, N. Dankbar, P. Kainz, E. Gedig, M. Vuyisich, C. Boozer, N. Ly, M. Toews, A. Uren, O. Kalyuzhniy, K. Lewis, E. Chomey, B.J. Pak, D.G. Myszka, A global benchmark study using affinity-based biosensors, Anal. Biochem. 386 (2009) 194–216, http://dx.doi.org/10.1016/j.ab.2008.11.021.
[18] E. Harlow, D. Lane, Using Antibodies: a Laboratory Manual, CSHL Press, 1999.
[19] W.D. Sikkema, An Fc-binding protein, Am. Biotechnol. Lab. 7 (1989) 42–43.
[20] D. Yang, A. Singh, R. Kroe-Barrett, Dataset of Binding Kinetic Rate Constants of Anti-PCSK9 Antibodies from Biacore T100, 2016. ProteOn XPR36, Octet RED384, and IBIS MX96 biosensor platforms., Data Brief. Submitted.
[21] R.B.M. Schasfoort, A.J. Tudos, Handbook of Surface Plasmon Resonance, Royal Society of Chemistry, 2008.
[22] R. Karlsson, P.S. Katsamba, H. Nordin, E. Pol, D.G. Myszka, Analyzing a kinetic titration series using affinity biosensors, Anal. Biochem. 349 (2006) 136–147, http://dx.doi.org/10.1016/j.ab.2005.09.034.
[23] W. Palau, C. Di Primo, Simulated single-cycle kinetics improves the design of surface plasmon resonance assays, Talanta 114 (2013) 211–216, http://dx.doi.org/10.1016/j.talanta.2013.04.022.
[24] D. Frenzel, D. Willbold, Kinetic Titration Series with Biolayer Interferometry, PLOS ONE 9 (2014) e106882, http://dx.doi.org/10.1371/journal.pone.0106882.
[25] Biacore AB, Biacore T100 product information sheet, (n.d.). https://www.biacore.com/lifesciences/products/systems_overview/system_information/index.html.
[26] Bio-rad, ProteOn XPR36 Protein Interaction Arrary System, (n.d.). https://www.bio-rad.com/en-us/applications-technologies/label-free-biomolecular-interactions.
[27] R. Tobias, Application note 14: Biomolecular Binding Kinetics Assays on the Octet Platform, (n.d.). http://www.fortebio.com/literature.html.
[28] IBIS Technologies, White Paper: Specifications of the IBIS MX96., (n.d.). http://www.ibis-spr.nl/inhoud/uploads/151015-WP1-Specifications-of-the-MX96.pdf.